THERMALLY ACTIVATED SULFURIZATION FOR $CuInS_2$ SOLAR CELLS

by

KARAN AGRAWAL

Presented to the Faculty of the Graduate School of

The University of Texas at Arlington in Partial Fulfillment

Of the Requirements

For the Degree of

MASTER OF SCIENCE IN MATERIALS SCEINCE AND ENGINEERING

THE UNIVERSITY OF TEXAS AT ARLINGTON

December 2007

Dedicated to my Parents
Vijai and Suresh

ACKNOWLEDGEMENTS

I wish to express my sincere gratitude and thanks to my advisor Dr. Michael Jin for giving me an opportunity of doing research under his guidance. This research is a result of his guidance and constant motivation. He also helped me a great deal in improving my presentation skills.

I sincerely thank Dr. Choong-un Kim for his support and for being my committee member. I would also like to thank Dr. Yaowu Hao for reviewing my thesis work and for being my committee member. I express my gratitude to all the professors and the department staff for offering their support whenever required, especially our secretary, Jennifer Standlee for helping me with ordering research supplies and helping me with my academic paperwork.

I appreciate the help of Dr. Nasir Basit who trained me on various equipments at Nanofab. I also would like to thank Dr. Jiechao Jiang for his support in using the characterization equipments at Characterization Center for Microbiology and Materials.

I appreciate the help of my colleagues and all the friends who motivated me and supported me during my thesis work. I thank Dr. Jeeyong Kim who helped me during the sputtering process in Materials Science Lab. I express my thanks to Dr. Xin Chen, who helped me during my setup at Chemistry Research Building. I thank Xin Wang, Chun-Young Lee, Chienwen Huang, Punnapob Punnakitikashem, Mark, Goeffery Gaban, Sean

Passes, Pankaj Hazarika, Puneet Saggar, Vaneet Sharma, Mitesh Joshi, Rashid Idnan Islam and Sachin Soni for their consistent support during my entire student career.

Finally I express my heartiest thanks to my parents and my brother for their love and affection that inspired me throughout the time.

October 11, 2007

ABSTRACT

THERMALLY ACTIVATED SULFURIZATION

FOR $CuInS_2$ SOLAR CELLS

Publication No. _____

Karan Agrawal, M.S.

The University of Texas at Arlington, 2007

Supervising Professor: Dr. Michael Jin

Chalcopyrite Solar Cells are now being fabricated on flexible (polymer) substrates. However, CuInS2 solar cells have not been fabricated on the polymer substrates on the commercial scale due the sulfurization temperature which limits the use of polymer substrates during fabrication. To overcome this problem a thermally activated sulfurization process for the manufacture of $CuInS_2$ solar cells from the Cu-In bilayers is described in this work. This sulfurization process can be employed for lower temperature for the formation of the absorber layer. For the sulfurization, the Cu-In bilayer with different compositions is prepared by thermal evaporation in which the In-rich film shows the presence of high $CuIn_2$ phase while the Cu-rich film shows the presence of high $Cu_{11}In_9$ phase. The films were sulfurized in a home built reactor. In this reactor, the

high molecular weight sulfur molecules are broken down into smaller rings at high temperature (600, 700 and 800^{o}C) and then reacted with the Cu-In bilayer at lower temperature (500^{o}C). The compositional analysis shows In loss during sulfurization which is expected due to the formation of In_2S_2 formation; and the EDS analysis shows the possible presence of Cu-S compound formation which are etched using the KCN solution. After etching the film shows more stoichiometric concentration of Cu, In and S elements. $CuInS_2$ film is prepared. In5s4 compound also forms in the film during sulfurization process.

The deposition method of CdS layer through chemical bath deposition has been discussed. The CdS layer forms the n-type layer for the p-n junction $CuInS_2$ solar cell. The details of the setup are discussed and the film is characterized for its transmittance using UV-VIS spectrometer. 90% transmittance is observed for approximately 50nm thick CdS film on glass. Indium tin oxide layer is studied as the windows layer for the $CuInS_2$ solar cell. Its properties are optimized using the sputtering equipment. Films with sheet resistance below 20 Ω/square have been prepared with the percent transmittance close to 90%.

TABLE OF CONTENTS

LIST OF ILLUSTRATIONS

LIST OF TABLES

PREFACE

The Thesis has been divided into three major sections:

1. Chapter 1 – Thermally Activated Sulfurization Scheme for $CuInS_2$ Sollar Cells.
2. Chapter 2 – Cadmium Sulfide Buffer Layer for $CuInS_2$ Solar Cell
3. Chapter 3 – Indium Tin Oxide Window Layer for $CuInS_2$ Solar Cell

The major focus of the thesis has been on the chapter 1 where most of the time has been spent. $CuInS_2$ thin layer was manufactured in a home build reactor setup. The film was characterized for its properties. In the second chapter, the chemical bath deposition setup of CdS has been discussed. The setup was prepared to learn how to deposit CdS and to complete the cell structure. In the third chapter, the properties of indium tin oxide layer prepared by sputtering process have been discussed. The film properties are optimized using the various characterization tools for better cell performance.

CHPAPTER 1

THERMALLY ACTIVATED SULFURIZATION FOR $CuInS_2$ SOLAR CELLS

1.1 INTRODUCTION

The availability of cheap sources of primary energy is a reliable indicator of the standard of living in any country of the world. Worldwide energy demand is predicted to keep growing with the world population and with the standard of living that can be afforded [1]. In today's world, fossil and nuclear fuels are the world's primary energy sources. The global resources of fossil fuels are limited and their consumption implies emission of the greenhouse gases like CO_2, which is of major concern since global warming seems to be emerging as a reality [2].

Solar energy provides the alternative source of primary energy. Solar cells when exposed to the sunlight produce electrical energy. They can operate continuously minimal maintenance. In order to achieve reasonable power level for consumers, many solar cells are connected each other to form commercial modules and they are typically guaranteed for 20 years or longer. The global market for solar modules has been growing at an annual rate of about 40 % for the past few years and is expected to sustain the growth for coming years. However, current contribution of the solar cell technology to the world

energy supply is still only about 0.003 % while other renewable energy sources contribute about 0.1%.

The environmental concern of solar modules is limited to their production and to their ultimate disposal. Concerning these criteria, solar cells have clear advantages over fossil and nuclear energy sources. However, on the other side, electric energy from solar cells is not price competitive with fossil and nuclear sources. Though the operation of solar modules is almost free of cost, but the high initial investment makes electricity from solar modules comparatively expensive. For solar cells to make significant contribution to the world energy, their electricity production has to be as cheap as that from other conventional sources. In this regard, two important parameters are the production cost of a module and its solar-to-electric power conversion efficiency. The maximum power which can be provided by a module when facing the unobstructed sun is simply the product of the solar input, the module area and its efficiency.

Solar cells have various applications, for example, virtually all space installations. Wafer-based single-crystalline III-V compound semiconductor solar cells power many of these space satellites. Though efficiency values above 30% are reached, however, it is very expensive. They are also used for terrestrial concentrator modules which work efficiently only in direct sunlight and requires a mechanical tracking system, leading to a demand for maintenance.

Wafer-based Si solar modules own above 90 % of the market. They are either made from single-crystalline or multi-crystalline wafers. Si technology has reached power conversion efficiency (PCE) of 25 % and commercial modules have reached 15 %.

Multi-crystalline wafers are cut from cast ingots which are produced more cheaply than single crystals, but they make less efficient cells. Both technologies require very high purity Si which is a major contributor to the total system cost.

Alternatively, great promise for cost-competitive solar modules lies in continuous in-line production. Many technologies involve the deposition of various layers of thin films onto a substrate that can be manufactured and coated by the mile rather than by the foot. Amorphous Si, CdTe and $CuInSe_2$-based alloys have been made in to the solar modules this way. PCE close to 20 % has been achieved with $Cu(In,Ga)Se_2$ (CIGS) solar cells on glass substrates. On the commercial scale, 11 % - efficient modules are available. There are also next generation photovoltaic devices like dye-sensitized solar cells and organic solar cells. Major challenges for these technologies are low PCE and long-term stability.

While wafer-based Si solar cells are considered as the first generation solar cells, thin-film solar cells are considered as the second generation of photovoltaic technology due to their higher cost-reduction potential compared to conventional Si modules. The cost advantages are due to lower material and energy consumption, lower semiconductor quality requirements, and monolithic integration capability. More recently, the thin-film technologies are boosted additionally by shortage in the supply of Si.

Thin-films based Cu-chalcopyrite absorbers represent the most advanced thin-film solar cell technology with laboratory cells reaching PCE above 19 % [3]. Modules of $Cu(In,Ga)(S,Se)_2$ solar cells have reached the production stage at several places

worldwide and large modules have reached efficiencies above 13 % [4] with output power of 80 W [5].

The basic structure of the solar cell is shown in the Fig 1.1, and the p-n junction is formed between the p-type chalcopyrite absorber and the n-type buffer layer, CdS. There are environmental issues concerned with the use of Cd in the cell. Hence, alternative Cd-free materials are under investigation [6].

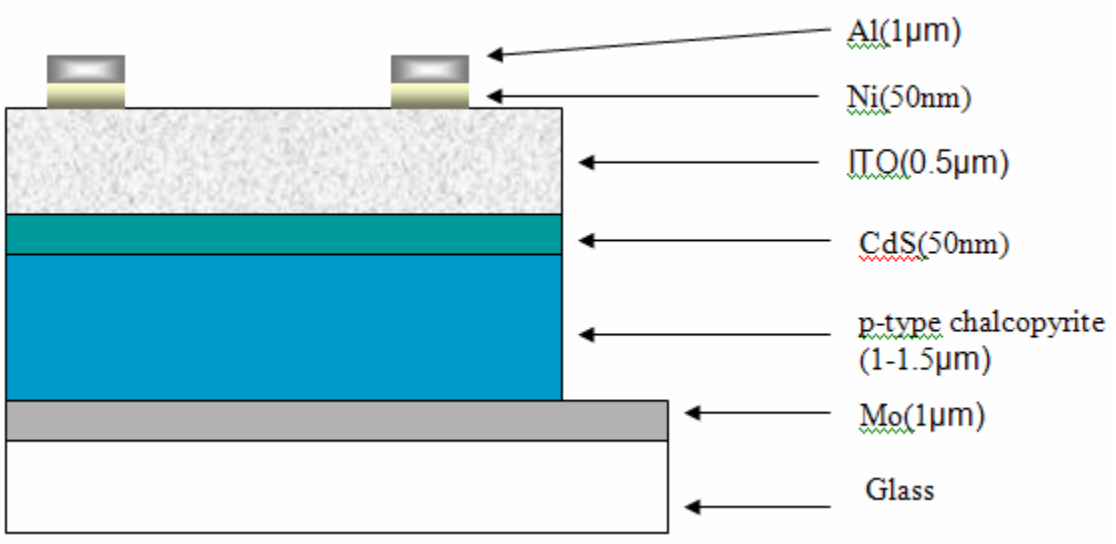

Fig 1.1: Basic layer structure of ITO/CdS/$CuInS_2$ heterojunction solar cell

About 1 μm thick molybdenum is typically used as the back contact. On top of the back contact, p-type chalcopyrite thin film is deposited as an absorber layer for the cell. To complete the p-n junction, CdS layer is deposited as the n-type semiconductor. Since CdS is very resistive, very thin (50 nm) layer is deposited compared to the p-type layer. Indium tin oxide (ITO) as the window layer on top of the CdS layer helps with

charge collection from the CdS layer. As the top contact of the cell, Ni/Al bi-metallic layer is often used - nickel acts as the adhesion layer between Al and ITO.

The major focus has been the $CuInS_2$ layer in this thesis. $CuInS_2$ is a promising candidate for thin film solar cells since it exhibits a direct bandgap of 1.5 eV, which results in nearly optimum theoretical PCE for solar energy conversion [5]. The higher bandgap results in higher open circuit voltage for $CuInS_2$, so there are less series connections necessary on a module for the same module electrical output. It also results in smaller thermal coefficient of the open circuit voltage of $CuInS_2$, therefore it has a smaller voltage decrease with increasing temperature. The currently available commercial technique for the deposition of large-area devices is a two-stage process in which a sequentially sputtered or thermally evaporated Cu-In bilayer or multilayer is transformed into $CuInS_2$ by means of reactive annealing (sulfurization). The sulfurization temperature is typically in the range of 500 – 600 ^oC. In numerous experimental studies, this two-stage process and the accompanying morphological and phase transformation of the Cu - In precursor layer are described [7-14].

In this study, we have manufactured the $CuInS_2$ layer by a thermally activated sulfurization scheme. All the sulfurization schemes which have been studied earlier involve high substrate temperature (500-600^oC) as a result of which there are not much options to use light weight substrates. Hence, an idea is proposed that the sulfurization can be done at lower substrate temperature if we thermally activate the sulfur molecules by bringing them to a higher temperature and then subsequently react them with the Cu-In bilayer which are kept at lower temperature. If low substrate temperatures can be

achieved to obtain the $CuInS_2$ layer then the polymer substrates or other light weight substrates like Krypton can be used for the solar cell preparation. In this method, we have first made the sulfur molecules more reactive by bringing it to a high temperature (600, 700 and 800 ^oC) and then subsequently sulfurized Cu-In bilayer which is kept at 500 ^oC. By bringing the sulfur molecules to the higher temperature, the higher molecular weight sulfur molecules are broken into the smaller molecules, thus, becoming more reactive. Hence, the sulfurization of the bilayer is expected to be achieved at comparatively lower temperature. Also, the experiment does not involve any vacuum process during sulfurization.

In this thesis the behavior of Cu-In bilayer prepared by evaporation has also been studied. Hence in the following sections, we have discussed the properties and background of the copper-indium bilayer and various compounds that are formed during the bilayer formation. After this, a brief background of $CuInS_2$ has been given, which also involves the different methods of making the absorber layer. Current knowledge on sulfur molecules in liquid and vapor phases has also been discussed.

1.1.1 Copper-Indium Bilayer

There have been some investigations before on the preparation of Cu-In precursor layer for the chalcopyrite solar cells [15]. Both ‘Cu on In’ and ‘In on Cu’ bilayers have been often deposited on molybdenum coated glass, and the ‘Cu on In’ bilayer has been preferred over the ‘In on Cu’ bilyer; its related to the morphological properties of the precursor films. The Cu layers evaporated onto Mo coated glass substrates at room

temperature have small grains and they form smooth and continuous layers with adequate adhesion to the Mo surface. After indium deposition, the Cu-In precursor layers are partially alloyed [85-87] and they adhere well to the substrate. 'Cu on In' bilayers give rise to more complete intermixing between the two elements since Cu is evaporated over an In layer which has a low melting temperature.

The recent work assessment of Cu-In phase diagram is of Bolcavage and co-workers [16] and Okamato [17]. The phase diagram is shown in the Figure 1.2. We see that, at room temperature, the stable phases of the Cu-In system are Cu, Cu_7In_3 (δ), $Cu_{16}In_9$ (η), $Cu_{11}In_9$, and In. In addition, $CuIn_2$ has also been observed which is not present in the phase diagram [17]. The melting point of In is 156 °C while $CuIn_2$ and $Cu_{11}In_9$ are thermally stable up to 148 ^oC [8] and 307 ^oC, respectively. Depending upon the exact composition, the $Cu_{16}In_9$ undergoes a phase transition between 307 ^oC and 389 ^oC.

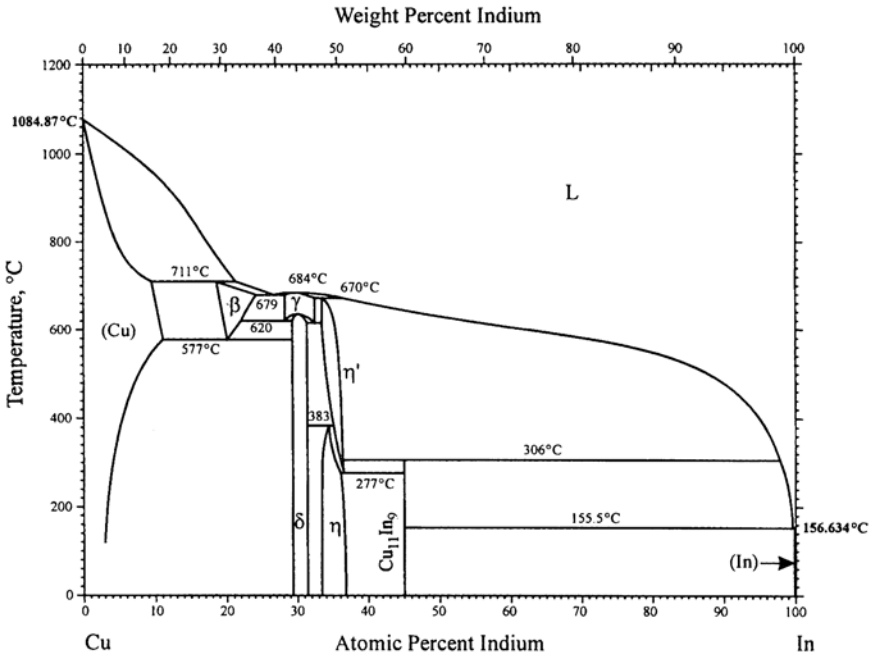

Figure 1.2: Cu - In phase diagram [17]

1.1.1.1 $CuIn_2$ phase

The $CuIn_2$ phase was first discovered by Keppner and co-workers [18] in perturbed angular correlation (PAC) experiments on sequentially evaporated thin Cu-In films, in which it forms via a solid-state reaction at room temperature. These authors identified an unknown phase via its PAC signal and determined the stoichiometry to be $CuIn_2$ through experiments with different overall compositions. At a later stage, $CuIn_2$ was shown as a bulk equilibrium phase of the Cu - In system [19] and additionally determined its temperature stability in thin films produced by sequential evaporation of the elements [8].

1.1.1.2 $Cu_{11}In_9$ phase

The first detailed investigation of $Cu_{11}In_9$ was reported in 1934 [20] in which it was found to exist at room temperature in a small composition range from 40.6 to 41.2 at %. In 1981, precise investigations were made to prove the existence of this phase between 43.5 and 44.5 at % [21].

1.1.1.3 $Cu_{16}In_9$ (η) phase

$Cu_{16}In_9$ region has been investigated extensively in the past because it is often observed during the annealing of the bilayer. Weibke and Eggers [20] found the phase stable up to 389 ^oC. Laves and Wallbaum [22] determined a partially filled NiAs type crystallographic structure of samples. Jain *et al*. [24] proposed a phase bundle of five phases around the composition of $Cu_{16}In_9$ phase; high-temperature hexagonal phase is of the partly filled NiAs type without any ordering of the structural vacancies. The four low-temperature phases are similar structure with vacancy ordering.

1.1.1.4 Cu_7In_3 phase

The phase was found by Weibke and Eggers to exist for In concentrations between 28.9 and 30.7 at% at room temperature [20]. It is stable from room temperature up to 630 ^oC [16,23]. The triclinic structure of Cu_7In_3 was found by Koster *et al.* in 1980 [25].

1.1.2 Copper Indium Disulfide Layer

$CuInS_2$ is a good candidate as photovoltaic absorber for the fabrication of high efficient and low cost solar cells. It has a direct bandgap energy of approximately 1.4eV which is in the optimum range for solar-energy conversion [26]. Various routes to prepare large-grain (> mm) polycrystalline (towards single-crystalline quality) $CuInS_2$ exist and many have been partially explored. The various growth methods include chemical vapor transport [27,28], melt growth including vertical Bridgman [29,30], growth at elevated pressure [31,32], and molecular beam epitaxy of heteroepitaxial thin films [33-35]. Early results yielded about 3 % PCE in photoelctrochemical solar cells using polysulfide [36]. Information on the phase relations in the Cu-In-S system was initially provided by Binsma in 1980 and 1981 [37,38]. The initial preparation of p- or n-type samples necessitates experience in doping of $CuInS_2$. Due to the relatively large homogeneity range, doping was thought to occur from stoichiometric deviations [38]. This is expressed by

$$\{(Cu]+3[In])/2[S]\}-1<>0, \quad (1)$$

where the brackets denoted the concentration of the elements constituents. It is implicitly assumed that doping occurs via interstitial point defects; in addition, the valence of the respective atoms has been taken into account and the energy levels of the interstitials have been assumed to be equal. In equation 1, the influence of different interstitial positions with different energetic is not included. It is known from photoluminescence and Brewster angle spectroscopy that these energies are not identical but differ quite substantially [39-41].

Figure 1.3 shows the ternary phase diagram of Cu-In-S system. There are tie lines between $CuInS_2$ and InS and In_6S_7. Another tie line exists between $CuIn_5S_8$ and In_6S_7. In the triangle $CuInS_2$-InS-In_2S_3, only the compound $In_{2.8}S_4$ is not connected by a tie line. An equilibrium tie lines between $CuInS_2$ and both $Cu_{11}In_9$ and In exist. The insert in the figure shows the detailed analysis of the homogeneity range of $CuInS_2$ in In-rich direction towards InS. The measurements yielded an upper limit for the homogeneity range of the compound $Cu_{1-x}In_{1+x}S_2$ ($X < 0.03$) indicating largely tolerated nonstoichiometry in this material.

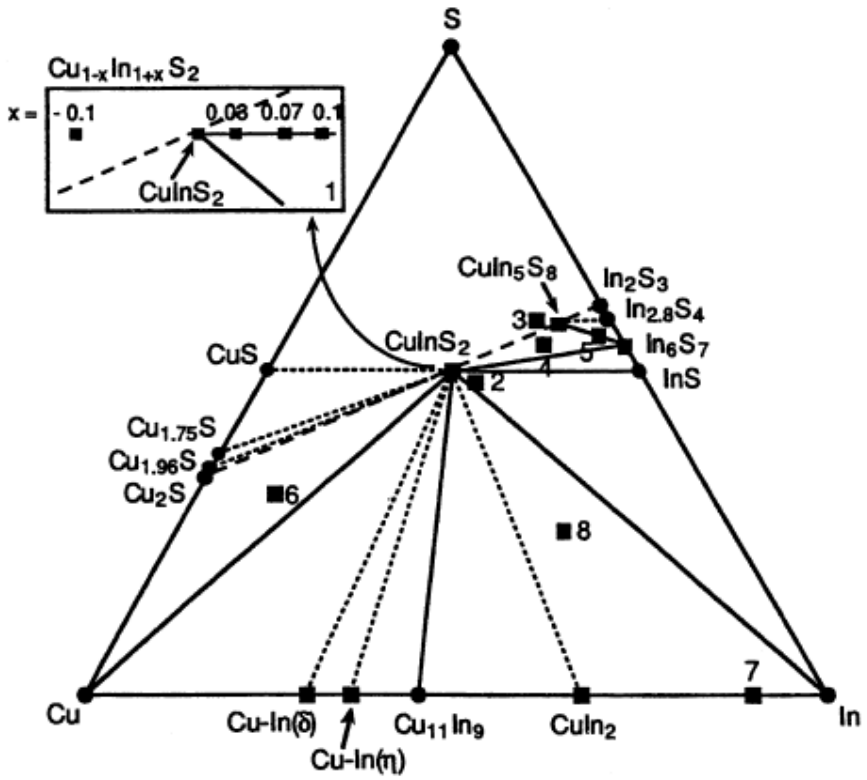

Figure 1.3: Gibbs phase triangle for the Cu-In-S system at room temperature including tie lines deduced from the combined XRD and PAC experiments [42]

There are several preparation methods which have been employed in different states of development for a systematic investigation of the material properties relevant for photovoltaic applications. The investigation is aimed to identify the suitable process for the growth of $CuInS_2$. The following preparation methods have been explored [43]:

1. Co-evaporation (simultaneous evaporation) of the elements similar to the technology used by ZSW and Würth Solar in Germany.
2. Sequential sputtering of metal films followed by annealing in sulfur vapor which can be two-step or sequential process. This is the current baseline technology of Hahn-Meitner Institute (Germany) which is comparable to the technology used by Siemens Solar GmbH (Germany) for $CuInS_2$ [44,45,46].
3. Sequential evaporation of metal films and sulfurization in H_2S, sulfur vapor, or an organic sulfur source [47].
4. Atmospheric pressure spray chemical vapor deposition [48,49].
5. Molecular beam epitaxy of Cu/In precursors on glass substrates and subsequent sulfurization in sulfur atmosphere [50].
6. Spray pyrolysis of both p- and n-type $CuInS_2$ [51,52].

In table 1, most commonly used two methods, the simultaneous (co-evaporation) and sequential evaporation techniques have been compared. The advantages and disadvantages of one over the other are given.

Table 1: Advantages and disadvantages of sequential and simultaneous techniques

Simultaneous evaporation (co-evaporation)	**Sequential evaporation**
Advantages: - Very high efficiency (number). - Growth can be influenced by controlling evaporation rates and substrate temperature: doping, phases, band gap engineering. - Multinary alloys possible and it needs only one vacuum chamber.	- Well scalable, and uses technology that is already available for large areas. - Stoichiometry and homogeneity can easily be controlled.
Disadvantages: - Exact control of stoichiometry is difficult. - Homogeneity on large areas requires complicated system layout.	- Primarily governed by thermodynamics of the system - concentration gradients and multinary alloys are always possible.

Hahn-Meitner-Institute uses sequential sputtering of the metals and rapid thermal annealing in sulfur atmosphere for the development of $CuInS_2$ layer [43], and they have achieved the world best active are PCE of 12.5 % (Figure 1.4).

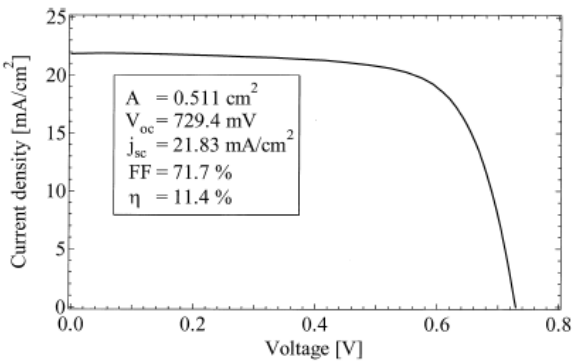

Figure 1.4: I-V measurements of the best RTP-$CuInS_2$ solar cell [43]

$CuInS_2$ mini-modules have been fabricated at the Hahn-Meitner-Institute, Germany [53]. The majority of these mini-modules are in the PCE range of 8 – 9 % with the best efficiency of 9.7 %. The module consists of seven series integrated cells with each cell having an open circuit voltage of 723 eV. The module has an open circuit voltage identical to those achieved with the good single cell devices while the module's fill factor and the short circuit current density are still lower than those of single cell devices.

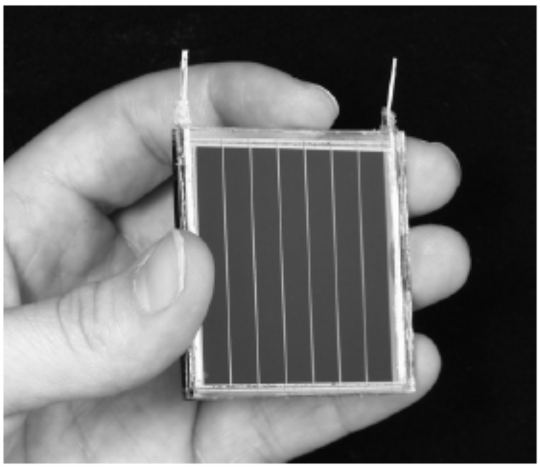

Figure 1.5: Encapsulated mini-module from $CuInS_2$ baseline manufactured at Hahn-Meitner-Institute, Germany [53]

There have been few studies on the Cu-poor $CuInS_2$ thin films. The studies done at the Hahn-Meitner-Institute show that the material quality is not suitable for solar cell applications [54] - poor material quality in terms of both crystal quality and electronic properties. Cu-rich films have grain size in excess of 1 μm whereas In-rich films have much smaller grains. Cu-poor thin films automatically generate a rectifying, buried junction.

A particular advantage of the Cu-S/$CuInS_2$ system is its tolerance to stoichiometric variation which is independent of the Cu to In ratio in a wide range (1.2 - 1.8). The Cu-S binary phases have been observed to form on the surface of Cu-rich $CuInS_2$ during sulfurization. It has been shown that this Cu-binary phase acts as a flux agent for the crystal growth of $CuInS_2$ (Klenk *et al.*, 1994 [55]; Scheer *et al.* 1995 [56]). The transformation of Cu_2S into CuS is expected to take place in the cool-down period at about 260 ^oC [57]. This transformation consumes more sulfur and requires a sulfur excess environment throughout the whole process. The sulfur excess environment can also be crucial for the complete segregation of the over-stoichiometric Cu within the absorber layer. Experiments have shown that sulfur acts as a scavenger for the excess Cu atoms [58], and that CuS completely segregates [59]. The CuS surface layer although of hundreds of nanometer thickness, does not form a full coverage but exhibits holes which expose the base $CuInS_2$ surface without CuS coverage [60]. Before preparation of the window layers, the CuS layer is required to be removed by KCN etching [60]. The KCN etching acts extremely selective on Cu-S phases where the etch rate is 5 orders of magnitude larger than the one of $CuInS_2$ [60].

There are still many aspects of the $CuInS_2$ solar cell which needs further research. For example, the photovoltage is limited to values around 750 mV which is only about one half of the bandgap. The cyanide etching and the presence of CdS are concern due to their toxiciy. Other aspects refer to the uncertainties concerning the state of the surface after the cyanide etching and the spatial variation of the surface condition. Also, the role of Na diffused from the underlying soda lime glass on the growth and the crystallization of $CuInS_2$, the presence of pinholes after fabrication and etching, and the influence of the chemical bath for deposition of CdS on the $CuInS_2$ still remain to be studied further.

1.1.3 Sulfur

1.1.3.1 General physical and chemical properties of sulfur

An allotrope of an element is defined as a solid phase (of the pure element) which differs by its crystal structure and, therefore, by its X-ray diffraction pattern from the other allotropes of that element. This definition can also be extended to microcrystalline and amorphous phases which may be characterized either by their diffraction pattern or by suitable molecular spectrum.

There is no other element which forms more solid allotropes than sulfur. At present, about 30 characterized sulfur allotropes are known. These can be characterized into ambient pressure allotropes and high-pressure allotropes depending on the conditions during preparation. The sulfur allotropes consisting of chains are less well characterized.

None of the allotropes melts without some decomposition [61]. Therefore, the melting point depends on the heating rate. The lower the heating rates, the lower the

melting point is observed since the decomposition products lower the melting temperature. Only in the case of S_8, a constant triple point temperature (115 ^oC) can be measured since the composition of the melt reaches the equilibrium after some time.

At room temperature, S_8 is the most stable form among various sulfur allotropes. Cyclo-octasulfur is stable as orthorhombic α–S_8. However, its conversion to monoclinic β-S_8 at temperature above the triple point of 96 ^oC is kinetically hindered and requires lattice defects or imperfections as present in a powder but usually not in a single-crystal [62]. Hence, single-crystal of α–S_8 usually melts at 115 ^oC without any conversion to the monoclinic form. The transition of orthorhombic to monoclinic sulfur depends on the heating rate and is often found well above 100 ^oC by differential scanning calorimetric measurements. Heating of S_8 to 90 – 110 ^oC, just below the melting point of 115 ^oC, does not result in any decomposition of the eight-membered ring, but as soon as the melt has formed, equilibration with other ring sizes takes place [63].

1.1.3.2 Sulfur vapor

Sulfur vapor, both saturated and unsaturated, have been investigated by UV-Vis spectroscopy [64], by resonance Raman spectroscopy [65-78], as well as by a sophisticated mathematical analysis [69] of carefully performed pressure measurements as a function of temperature and total sulfur concentration [70-72]. The sulfur vapor consists of all molecules from S_2 to S_8 under temperature and pressure-dependent equilibria. The presence of even larger molecules such as S_9 and S_{10} in equilibrium sulfur vapor has been observed [65]. Sulfur atoms can be expected in sulfur vapor only at

extremely high temperatures (> 2000 K) owing to their high enthalpy of formation of 277 kJ/mol [63].

Many authors have tried to derive the enthalpies of the gas-phase reactions as well as the entropies of the several S_n molecules (n = 2 – 8) from the temperature dependence of the mass and Raman spectra in combination with the total pressure of saturated or unsaturated sulfur vapor. These results are summarized in Table 2. The assumption most authors made was that only one species is present for each molecular size; in other words, possible isomers were neglected.

Table 2: Reaction enthalpies, ΔH_o (kJ/mol) for the gas-phase equilibrium reaction, cyclo-$S_8 \leftrightarrow 8/n\ S_n$ at selected temperature according to various experimental investigations

Temperature	298K	298 K (2^{nd} Law)	298 K (3^{rd} Law)	400K	400K	435-669K
$S_8 \leftrightarrow 4S_2$	420	404	387	393	414	405±9
$S_8 \leftrightarrow 8/3\ S_3$	275	253	231	251	255	257±11
$S_8 \leftrightarrow 2S_4$	190	150	137	172	234	169±13
$S_8 \leftrightarrow 8/5\ S_5$	73	90	77	96	96	85±13
$S_8 \leftrightarrow 4/3\ S_6$	34	48	34	35	35	35±2
$S_8 \leftrightarrow 8/8\ S_7$	28	28	20	27	28	28±2
Reference	[69]	[76]	[76]	[73]	[74]	[75]

The most detailed compositional analysis of sulfur vapor was published by Rau *et al.* in 1973. They measured the pressure of saturated sulfur vapor up to 1273 K. The densities of saturated and unsaturated sulfur vapor in the temperature range of 823 - 1273

K were analyzed. Using literature data for the entropy of S_8, they calculated the partial pressures of the molecules (S_2 - S_8) as a function of total pressure and temperature. The reaction enthalpies for the equilibria are listed in Table 3. The absolute concentrations of the various sulfur species in the saturated vapor at 500 ^oC (0.2 MPa) were calculated from the data of Rau *et al.* [69]. The data is given in Table 4.

Table 3: Concentrations of the various sulfur species (mmol/l) in the saturated vapor at 500 ^oC, calculated form the thermodynamic data of Rau *et al*. [69]. Total pressure is 0.2 MPa. The molar ratio (c) is normalized to the concentration of S_8; c(S_8) = 100

Species	Concentration (mmol/l)	Molar ratio
S_2	1.58	15
S_3	0.41	4
S_4	0.34	3
S_5	0.91	9
S_6	8.13	77
S_7	9.58	91
S_8	10.5	100

From table 2 and 3, we see that even lower molecular weight compounds are present in the vapor phase of sulfur at 0.2MPa pressure. Hence, we if increase the temperature further, it is possible to obtain more concentration of lower molecular weight species which shall be more reactive than higher molecular weight species.

1.2 EXPERIMENTAL SETUP

As the first step towards the development of low-temperature $CuInS_2$ solar cells, the copper and indium layers are deposited on glass first and sulfurized in the thermally activated sulfur atmosphere in this study. In this section, the experimental procedure for the preparation of Cu-In bilayer on glass is given. Also, the home-built sulfurization setup details have been discussed including the method of sulfurization. The various characterization techniques used for the characterization of the bilayer and the sulfurized samples thin films are provided.

1.2.1 Sulfurization setup

For the sulfurization of copper-indium bilayer, a home-made Chemical Vapor Deposition (CVD) reaction chamber is built. The schematic diagram of the equipment is shown in Figure1.6.

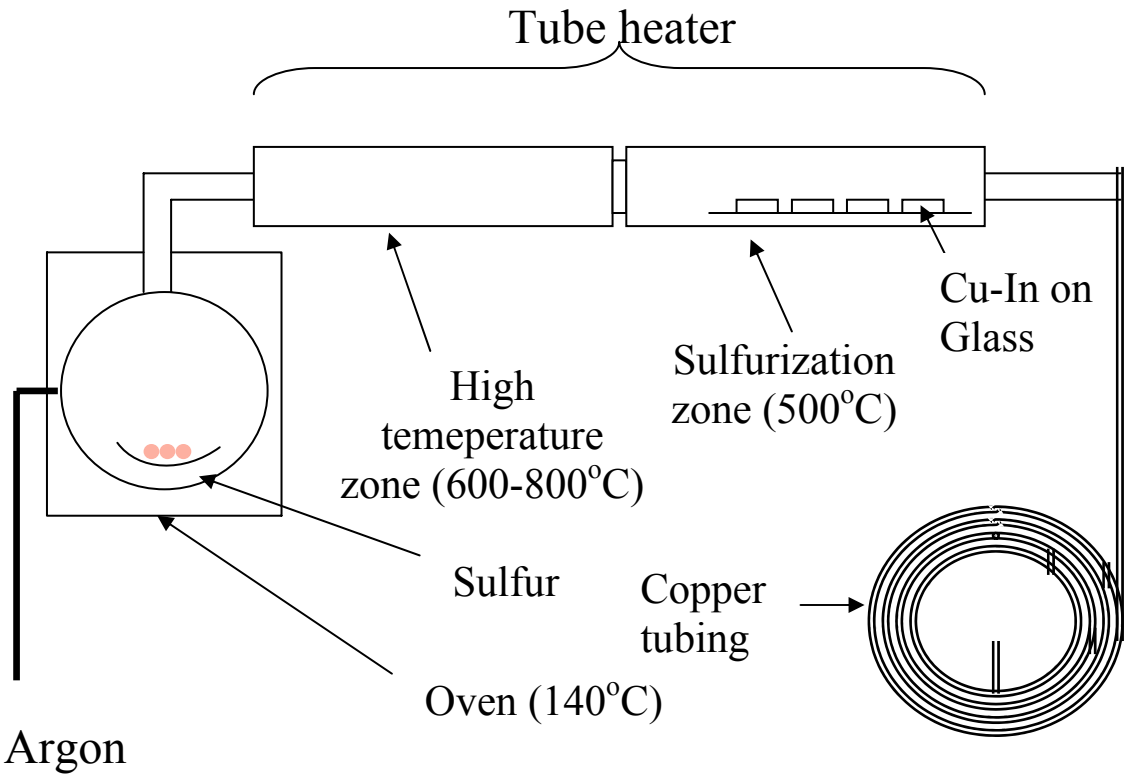

Figure 1.6: Schematic diagram of the sulfurization setup

The setup mainly consists of 3 parts;

1. Oven (evaporation zone)
2. Hot temperature zone (HT zone)
3. Sulfurization zone (SZ zone)

The gravity-convection oven (Baxter) has a chamber (16" x 16" x 16") with the heating element on the bottom and a port for a thermometer on top. The temperature of the oven can reach 140 °C in about 40 minutes. The purpose of oven is to evaporate the elemental sulfur - the melting point of sulfur is 120 °C). Hence, in the oven, sulfur is brought to its melting point and the vapor formed in the chamber is carried away by the argon. The sulfur vapor then passes through the glassware to the HT zone. To prevent

cooling of the vapor, the glassware between the HT zone and the oven is wrapped by the heating tape to keep the glassware above the melting point of sulfur so that no deposition shall take place in between. The temperature of the glassware was set to 240^{o}C. A picture has been shown in figure 1.7 showing the glassware arrangement and the sulfur placement inside the oven. A picture of the glassware (Figure 1.8) shows the connection between the oven and the tube heater.

Figure 1.7: Glass arrangement inside the oven and sulfur placement inside it

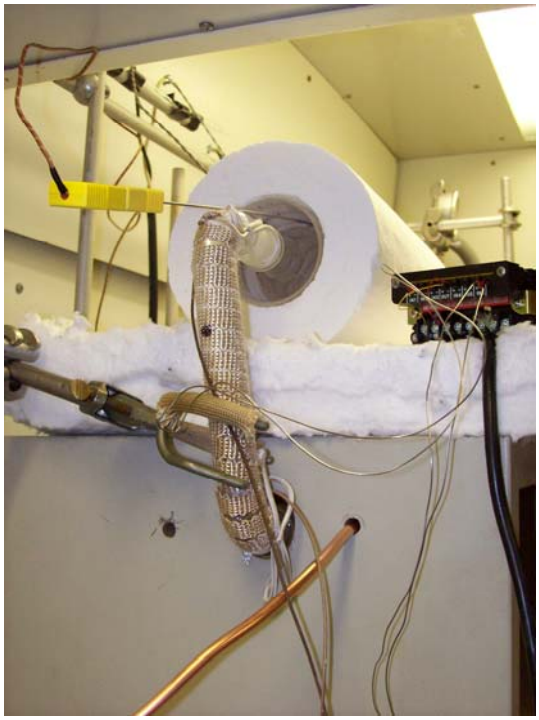

Figure 1.8: Sulfurization setup showing the glassware connection between the oven and the tube heater (HT zone)

Both the HZ and SZ are equipped with the same type of fiber-insulated tube heater (Zircar Ceramics, Item # CX15180A) which can be powered up to 1200 W. The two tube heaters (inner diameter:3 inch) are right next to each other, and a number of quartz tubing parts are connected through the tube heaters. The length of each tube heater is 1' (Figure 1.9) and narrow part of the connection inside the tube heater has a diameter of about 1" (Figure 1.10.). K-type thermocouples were purchased from Omega (Part #KQXL-116G-12) to monitor the temperature of the two zones. The thermocouples were placed inside the tube heater, but outside the actual reaction quartz tubing part in which argon and sulfur flow as shown in the figure 1.10.

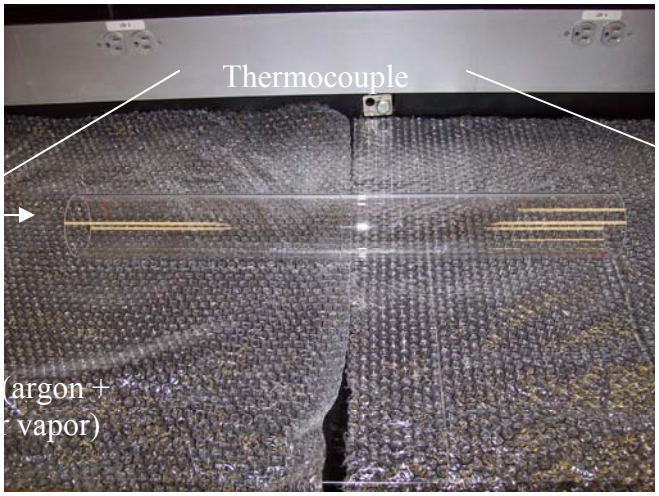

Figure 1.9: Quartz parts employed in the tube heater for sulfurization

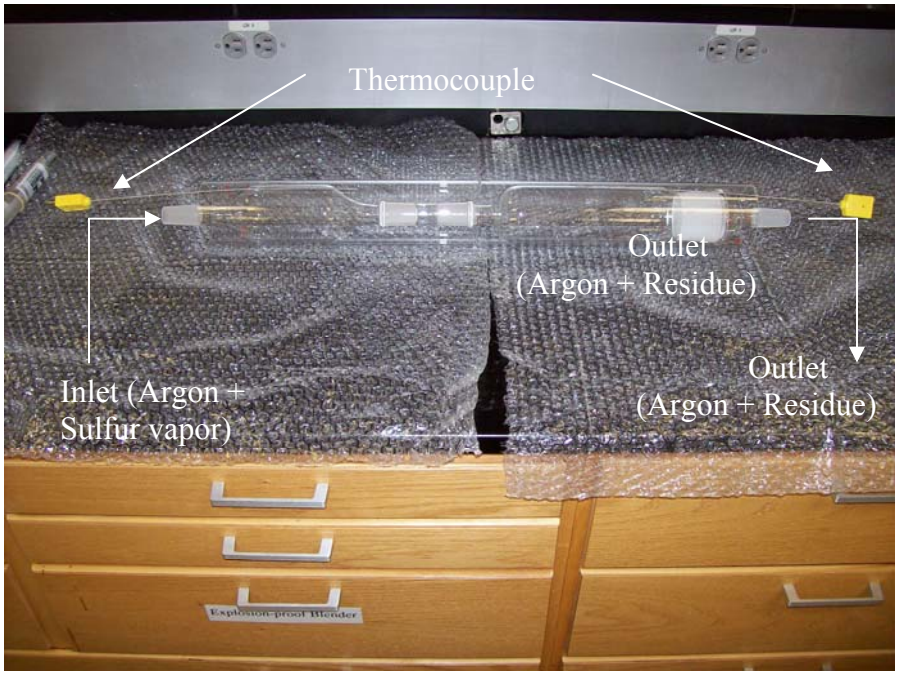

Figure 1.10: Quartz parts employed in the tube heater for the sulfurization

The picture of the tube heater is shown in Figure 1.11. At the exit of the tube heater, a pressure gauge is installed (shown in figure 1.12) to see if there is any pressure rise in the setup during the process.

Figure 1.11: Tube heater

Figure 1.12: Experimental setup showing the pressure gauge at the exit of the tube heater

The end part consists of the very long (approximately 12 feet) copper tubing which is rolled and its opening at the end is open to atmosphere.

After the sulfurization step, the samples are etched in the KCN solution for the removal of Cu_xS compounds in the film. A 10 wt % aqueous solution is prepared for KCN. The samples are etched in the solution for 2 minutes. Then they are washed in the DI water for 1 minute. The samples are blown dry with nitrogen.

1.2.2 Experimental Procedure

1.2.2.1 Cu-In bilayer formation

3" x 1" glass slides from Corning Glass Works (Cat. Number 2947) were used as substrates and they were cut into three 1" x 1" pieces before use. Then, the pieces were cleaned with a diluted Versa soap solution (Fisher). They were followed by further cleaning in the ultrasonic bath using toluene, acetone, and isopropyl alcohol for 20 minutes. The substrates were stored in tin boxes for later use.

The copper-indium bilayers are deposited sequentially on the glass substrates using thermal evaporator (NRC). Tungsten boats were used for the evaporation of the both elements. The base pressure of the chamber was attained to 6×10^{-6} torr before the start of the experiment. Quartz crystal was used to monitor the deposition rate of copper-indium on glass. Indium is often deposited first on glass and then copper was evaporated on the top of indium. This is done because Copper melting point is very high as compared to Indium; as a result of which if Copper is deposited first then the Glass

surface can be damaged by copper. The evaporation was done in such a manner so as to obtain the desired Cu/In ratio. Five batches of Cu-In bilayers on glass with different Cu/In ratio were prepared through evaporation for this study. Samples in the same batch have the same Cu/In ratio. The deposition rate for the copper and indium layers was maintained at low deposition rate of 1 -2 Å/s to avoid any undesirable pin hole formation.

The films were characterized for the thickness using the KLA Tencor profilometer. The X-Ray Diffraction (D500) was used to find the various compounds formed during evaporation. Glancing angle X-ray diffraction was performed to study the phases formed on the surface of the film. JEOL JEM 845 Scanning Electron Microscopy (SEM) equipped with Energy Dispersive Spectroscopy (EDS) was used to make compositional analysis of the samples.

1.2.2.2 Reactive sulfurization of the Cu-In bilayer

One sample is taken from each batch selecting total of five samples. They are analyzed for their composition, thickness, and the various phases that are present in the films. Then, each sample is cut into 4 small pieces. For one 'batch of sulfurization', one small piece is taken randomly from each sample thus, total of 5 pieces are selected for the single run of sulfurization (Figure 1.13). Three batches of sulfurization were created to perform sulfurization at three different HZ temperature.

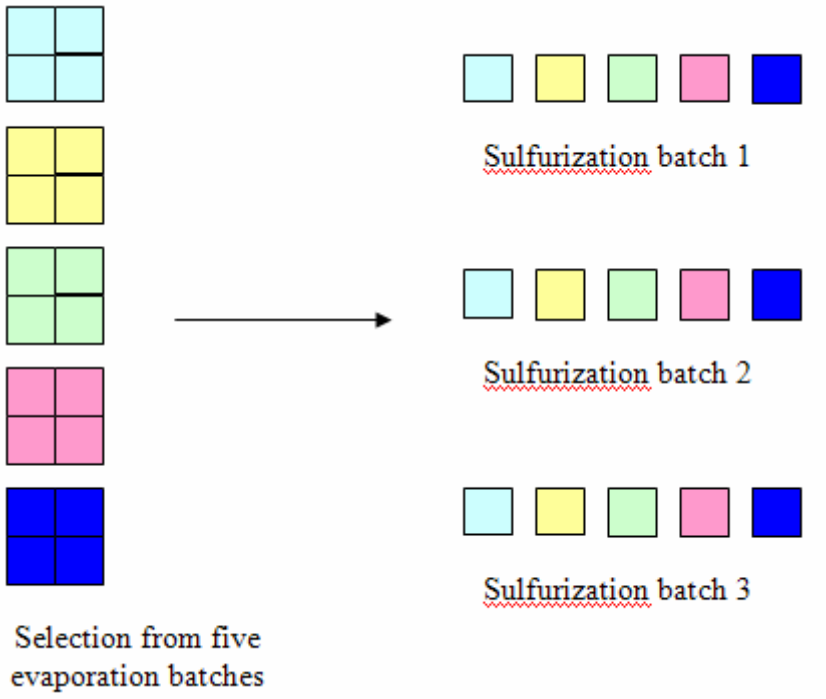

Figure 1.13: Preparation of samples for the sulfurization

Samples are placed over a quartz plate inside SZ. The temperature in the middle of SZ is maintained at 500 ^{o}C. The samples are placed in such a way that the sample closest to HZ is at the center of the SZ. The rest of the samples lie behind it in a line. The distance between the samples is approximately 2 – 3 mm.

As the source of sulfur vapor needed, 4 g of elemental sulfur powder is taken into a Pyrex petri dish which is placed inside the three neck flask. The flask is in the oven. One of the openings of the three necks is closed with the stopper while through another opening copper tubing is attached as the inlet of Ar gas. The other opening is saved for the extra gas line, and did not use in this study. The system is first purged for one hour

with argon to drive most of the atmospheric gases out of the system. After one hour, the oven is turned on. The temperature profile of the oven is shown in the Figure 1.14.

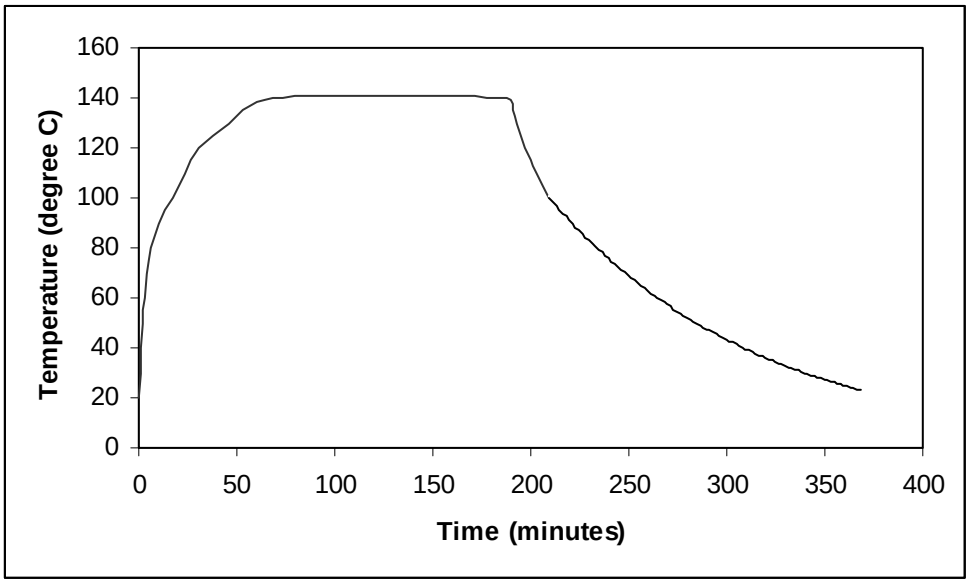

Figure 1.14: Temperature profile of oven during experimentation

After 30 minutes from the beginning, the oven temperature reaches the melting point of the sulfur, i.e. 120 ^{o}C. When the melting point of sulfur is reached, the HZ and SZ tube heaters are tuned on together. This is done so that the ramping shall occur under sulfur atmosphere preventing the oxidation of the film. The temperature profile of the HZ and the SZ are shown in the Figures 1.15 and 1.16.

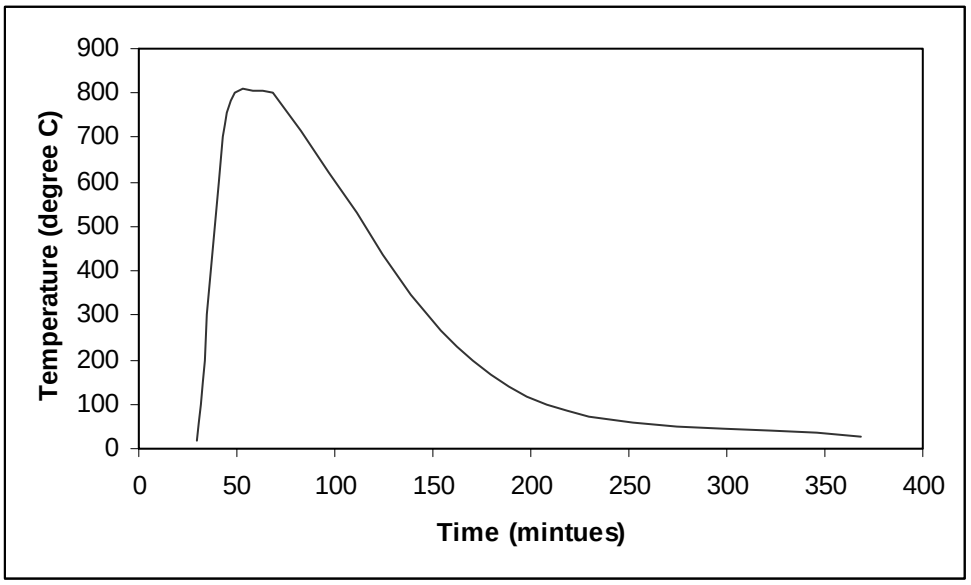

Figure 1.15: Temperature profile for Hot Zone

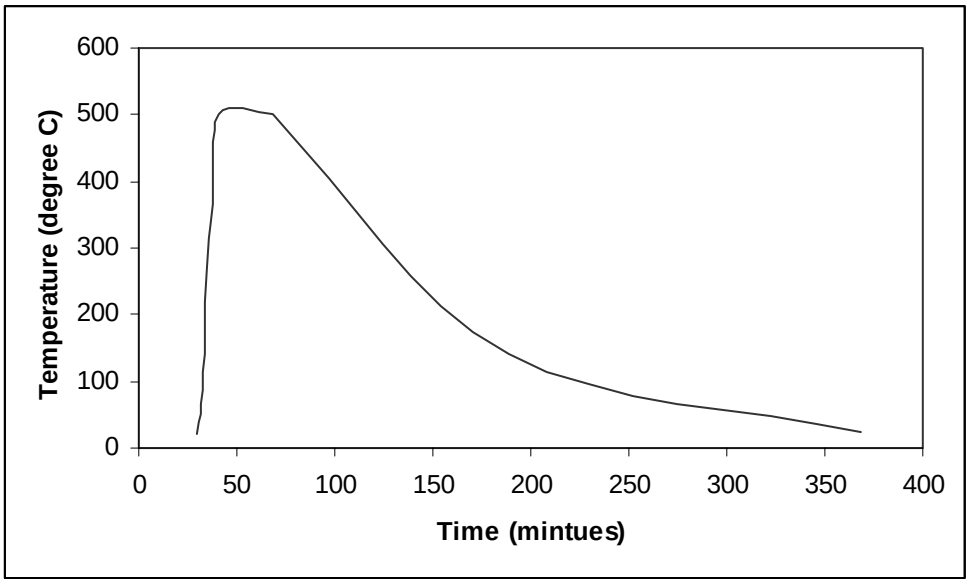

Figure 1.16: Temperature profile for Sulfurization Zone

It takes approximately 11 minutes for SZ to reach its temperature of 500 ^{o}C. The SZ temperature is kept constant for all the experiments. It takes about 18 minutes for HZ

to reach its value of 800 ^{o}C. The HT temperature was set at different temperatures for the three differenct 'batches of sulfurization' i.e., 600 ^{o}C, 700 ^{o}C and 800 ^{o}C for three different experiments. There is approximately 1 minute increase in ramping time whenever HZ temperature increases by 100 ^{o}C. The SZ is kept at fixed temperature, i.e. 500 ^{o}C, for all the experiments. The argon flow rate was controlled by a mass flow controller (MKS) and its value is set to 100 SCCM throughout the experiment and the power supply to the tube heaters were synchronized with a thermocouple (K-type) to control the temperature.

After 20 minutes since HZ has reached its maximum value, the HZ and the SZ are turned off together. As a result, the HZ and SZ temperatures start falling exponentially while the sulfur is still flowing. After 2 hours, the all temperatures reach about 140 ^{o}C. So, when the HZ and SZ temperatures are equal to that of the oven, the oven is turned off. It takes another 3 hours for the HZ, SZ, and oven to reach the room temperature. During this process the flow of argon is kept on at all times at 100 SCCM.

After the samples are sulfurized, SEM (ZEISS Supra 55 VP) is used to do the EDS analysis of the films and also to see the grain structure of the films. XRD (manufacturer?, D500) is performed to study the various phases formed in the film. After the preparation of the $CuInS_2$, the films were etched in KCN solution to remove the Cu_xS phase from the surface. Four samples were subjected to etching to see the properties of the film; 2 samples from batch 2 and two samples from batch 4 prepared at 700^{o}C and 800^{o}C were taken since these two have different Cu/In ratios as discussed ahead in the

results and discussion section 1.4.The films were analyzed again using EDS and XRD to see any change after etching.

1.2.3 Thermodynamic Calculation

Calculations of free energies were performed for the formation of the $CuInS_2$ compound with the elemental compounds. Also, possible mechanism of indium loss has been investigated through these calculations. Thermodynamic data necessary to calculate for the Gibbs free energy change (ΔG) was collected from JANAF compilations [93], Mills Compilation [94], and other references [95-99]. We use kJ /mol and kJ/mol·K as units of measure. Based on the 3rd law of thermodynamics, the free energy changes in a reaction r at a temperature T (Kelvin, K) is given by

$$\Delta_r G^o_T = \Delta_r H^o_{298} + T(\Delta_r\{(G^o_T - H^0_{298})/T\}).$$

As normally the Gibbs free energy function $-(G^o_T - H^0_{298})/T$ is tabulated, the equation can be rewritten as

$$\Delta_r G^o_T = \Delta_r H^o_{298} - T(\Delta_r\{-(G^o_T - H^0_{298})/T\}).$$

1.3 CHARACTERIZATION TOOLS

In this section various characterization tools have been discussed which have been employed during the thesis work.

1.3.1 UV/VIS/NIR spectroscopy

Figure 1.17: Perkin Elmer UV-Visible-NIR Spectroscopic unit

Ultraviolet-visible-near infrared spectroscopy involves the spectroscopy of the photons and spectrophotometry. It uses light in the visible and adjacent near ultraviolet (UV), and near infrared ranges. In this region of energy space molecules undergo electronic transitions. It is routinely used in the quantitative determinations of solutions of transition metal ions and highly conjugated organic compounds. In this study, Perkin Elmer UV-Visible-NIR Spectrometer Lambda 19 unit has been used for the investigation of the percent transmittance of the Indium Tin Oxide samples and CdS samples which are discussed in Chapter 2 and 3.

1.3.2 KLA Tencor profilometer

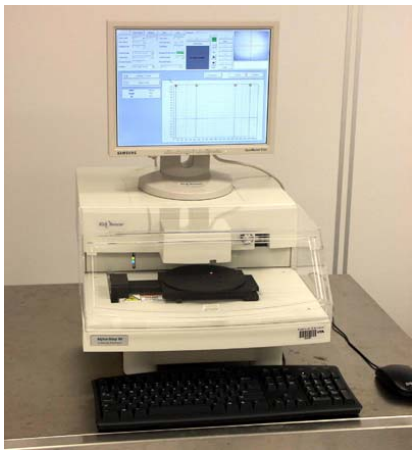

Figure 1.18: KLA Tencor profilometer with 400 micron vertical range

A profilometer is a measuring instrument used to measure a feature's length or depth, usually in the micrometer or nanometer level. A stylus is moved vertically in contact with a sample and then moved laterally across the sample for a specified distance and specified contact force. It can measure small surface variations in vertical stylus displacement as a function of position. This instrument has been used to measure thicknesses of the films across a trench in the film.

1.3.3 ZEISS Supra 55 VP scanning electron microscope

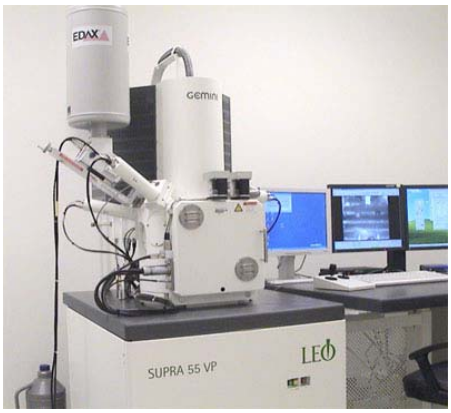

(a) (b)

Figure 1.19: (a) ZEISS Supra 55 VP SEM instrument and (b) JEOL JEM 845 SEM

ZEISS Supra SEM machine is equipped with the EDAX 4000 electron dispersive analysis system. It has a 1 nm resolution and it can accommodate the maximum of 8" wafer. It has the image nano devices with the latest in X-ray microanalysis. It is customized to study MEMs and NEMs devices. This has been used in this research to investigate the grain size of the films and also for the quantitative analysis of the elements present in the film. JEOL JEM has been used primarily to investigate the chemical composition of the elements and to see the morphology of the films.

1.3.4 NRC thermal evaporator

Figure 1.20: NRC thermal evaporator

The vacuum thermal evaporator technique thermally evaporates different materials to deposit them as thin films on substrates. Usually low pressure (about 10^{-6} ~10^{-5} torr) is needed to acquire necessary vapor pressure and to avoid any undesirable thermal reaction of the materials. NRC thermal evaporator has three-sources and it can coat up to seven wafers with a diameter of 3" or less in one run. This equipment has been used in this research for the deposition of metal layers like copper, indium, and aluminum.

1.3.5 Vecco four-point probe

Figure 1.21: FPP-5000 four-point probe

Four point probe system measures the sheet resistance, resistivity, and the thickness of a wide range of materials. This instrument has been used to find the sheet resistance of ITO films.

1.3.6 D-500 X-ray diffraction

Figure 1.22: D-500 X-ray diffractometer

In X-ray diffraction, a single beam of X-rays are diffracted from a single crystal X-Ray diffraction. It can determine the positions of most atoms in a crystal structure to within a few tenths of an Angstrom. It can be used on metals or minerals or engineered semiconductors or crystals of biomolecules such as aspirin or proteins. In this work, this equipment has been used to identify the various compounds and elements present in the film. It has also been used to find the relative amount of compound in the film.

1.3.7 RF/DC magnetron sputter

Figure 1.23: RF/DC magnetron sputter

Magnetron sputtering is a type of physical vapor deposition processes whereby atoms in a solid target material are ejected (sputtered) into the gas phase due to bombardment of energetic ions typically from plasma. It is commonly used for thin-film deposition, as well as analytical techniques. Standard physical sputtering is driven by momentum exchange between the ions and atoms in the material, due to collisions. This equipment is primarily been used for the deposition of ITO on Glass.

1.4 RESULTS AND DISCUSSION

The EDS analysis of the Cu-In bilayer prepared on glass through evaporation is shown in the Figure 1.25. One data point refers to one sample only, and EDS was performed in many different locations within each sample. The EDS results show that there is variation of composition for individual sample from the batch since the evaporation of the element is not uniform in all the directions. Also, the figure shows that the Cu to In ratio gradually changes between 0.9 and 1.1 - the batches 1 and 2 give the ratio close to 0.9 and the batches 4 and 5 give the ratio close to 1.1. The batch number 3 has the ratio close to 1.0. The thickness data of the Cu-In bilayers prepared in different batches is obtained with the profilometer and given in Table 4.

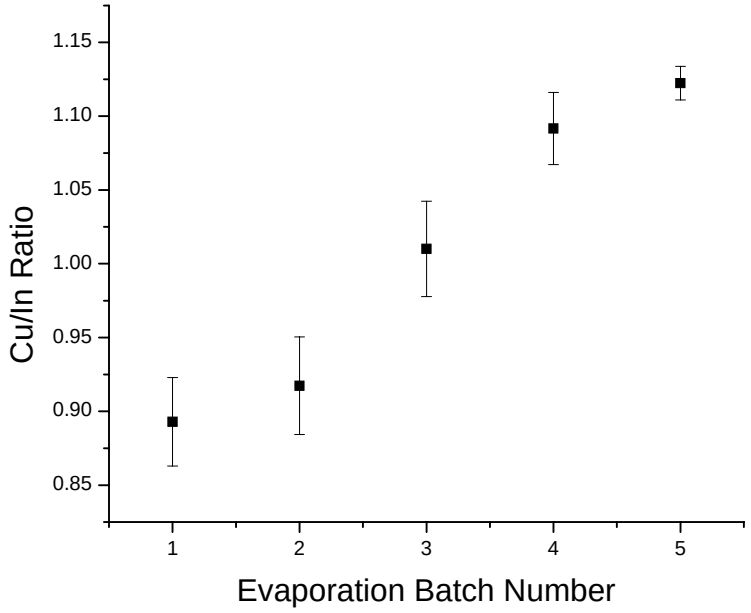

Figure 1.24: EDX analysis of Cu-In bilayer samples prepared from evaporation

Table 4: Thickness of the samples prepared from different evaporation batches

Evaporation batch number	Thickness (μm)
1	1.54
2	1.62
3	1.74
4	1.85
5	1.95

Figures 1.25, 1.26 and 1.27 show the XRD spectra of the bialyer for batches 1 to 5. In the figures, we do not see Cu peaks in any sample though Cu is deposited over In. On the contrary, In peak(s) can be found in all the samples. Also, In-rich films have high intensity peaks of $CuIn_2$ and In while a very small $Cu_{11}In_9$ peak. On the other hand, the Cu-rich films show a high intensity peak of $Cu_{11}In_9$ while lower intensity peaks of $CuIn_2$ and In. Hence, we can deduce that as the Cu/In ratio increases, the relative concentration of $CuIn_2$ and In decreases while that of $Cu_{11}In_9$ increases. This can be attributed to the more number of Cu atoms participating in Cu-rich phase ($Cu_{11}In_9$) formation. It should be also noted that $CuIn_2$ phase together with elemental Cu phase have been often observed as a dominant phase in Cu-rich films made by sputter [58]. It is thought that for thermal evaporation, the temperature of the film during the deposition process is at higher temperature than that of sputter promoting the formation of the high temperature phase ($Cu_{11}In_9$) as discussed in Introduction. Certainly, we see more of $CuIn_2$ phase for In-rich film because of the composition of the film. As discussed in Introduction, $CuIn_2$ phase has been known to form at room temperature [57]. However, there has been no study to explore how the phase of Cu/In bilayer changes from $CuIn_2$ to $Cu_{11}In_9$ as Cu to In ratio changes.

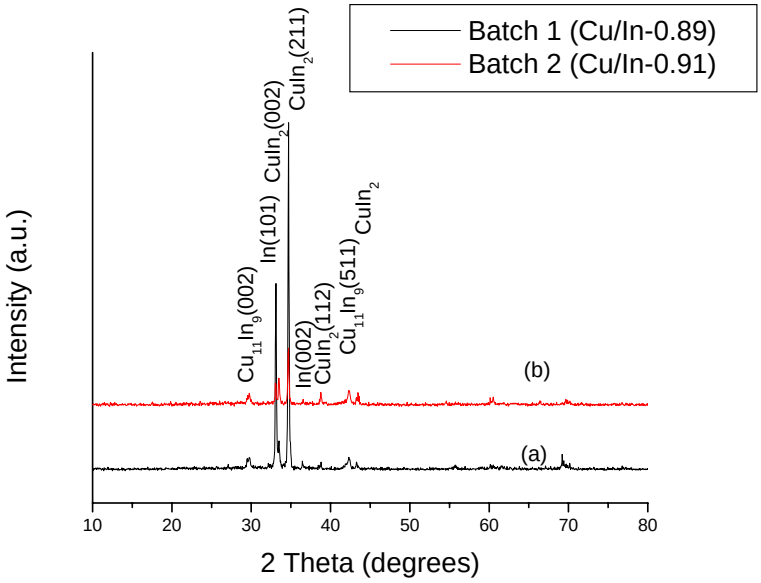

Figure 1.25: XRD spectra of evaporation batches 1 and 2

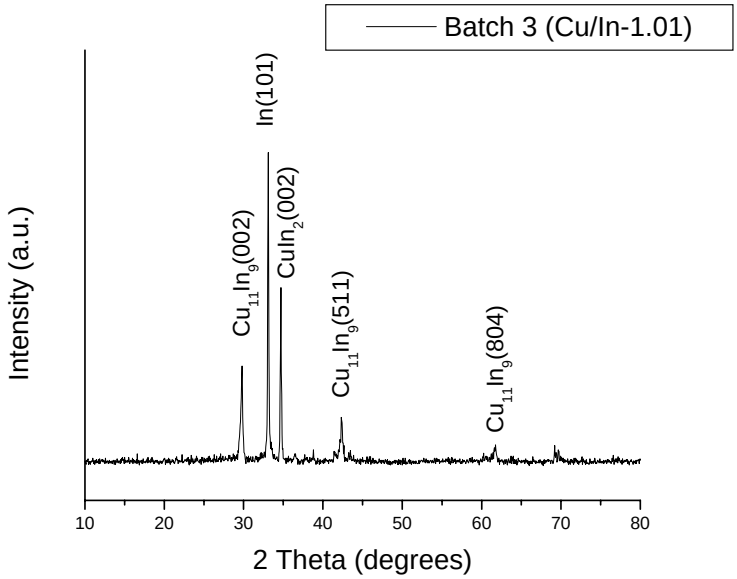

Figure 1.26: XRD spectra of evaporation batch 3

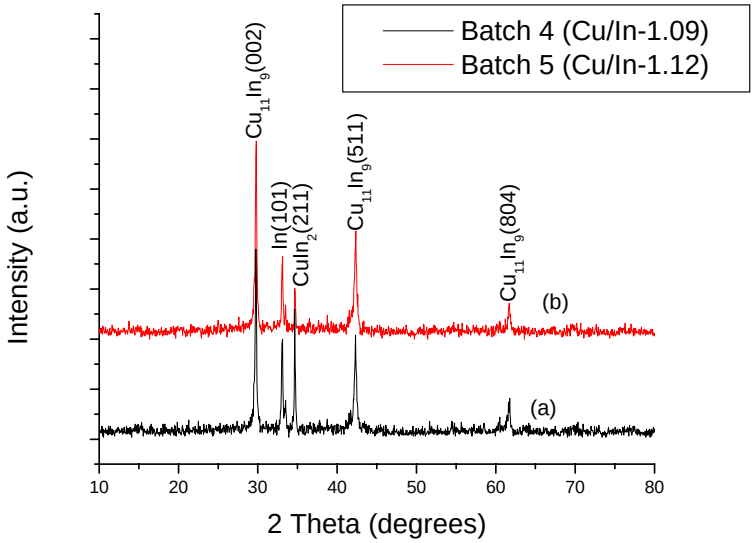

Figure 1.27: XRD spectra of evaporation batches 4 and 5

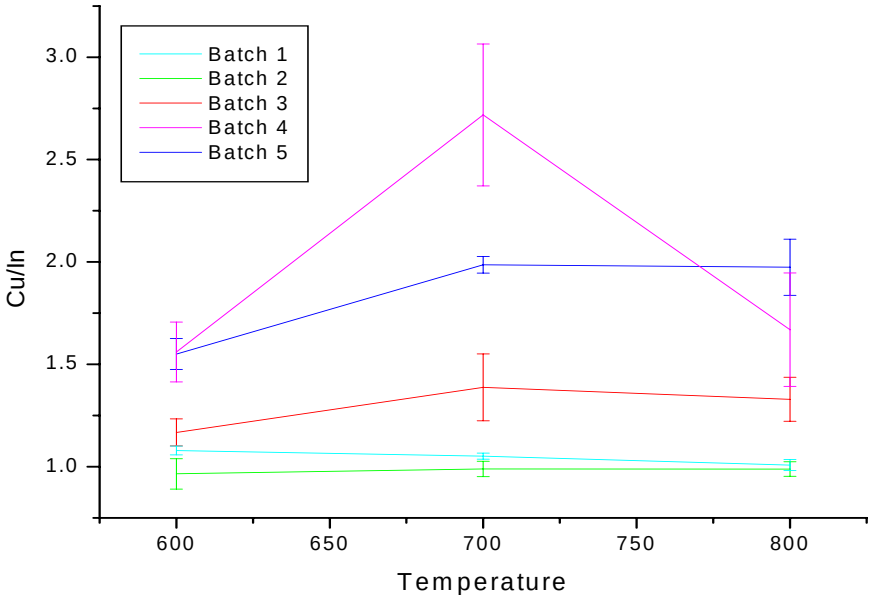

Figure 1.28: Cu/In ratio at 600, 700 and 800 ^{o}C after the sulfurization of the samples

After sulfurization, the relative concentration of Cu and In changes as the function of Temperature as shown in the Figure 1.28. From the figure the Cu/In ratio does not remain same as it was before sulfurization. Although In loss has been observed before during sulfurization [10] at 600^{o}C, for the Cu-rich samples, there is tremendous In loss (specially at 700^{o}C and 800^{o}C) while for the In-rich samples, the change is not much with respect to temperature. There is less In loss for In-rich samples compared to the Cu-rich samples. The Cu/In ratio remains between 0.9 and 1.1 for all temperatures for In rich samples. However, for the batch 3 (Cu/In=1.0), there is comparatively more In loss especially at temperature over 700 ^{o}C. The batches 4 and 5 (Cu/In=1.1) experiences even further In loss at high temperatures. For the batch 4, we see that the In loss is highest at 700 ^{o}C while it gets lower at 800 ^{o}C. However, for other samples, the In loss is almost same between 700 ^{o}C and 800 ^{o}C. We also observe that there is high In loss at higher temperature which can be attributed to the more In_2S_2 formation due to the availability of more reactive sulfur species (the thermodynamic calculations for this are shown at the later stage in this section). We also see that for the sample from batch 4, the data composition goes up at 700^{o}C and then down at 800^{o}C; however there is also maximum variation of composition in the sample which can be attributed to noise level.

Data explains that the In loss increases as the Cu/In ratio increases in the film. Since, In-rich samples show higher relative concentration of $CuIn_2$ phase, it is possible that the $CuIn_2$ phase prevents the In loss during the sulfurization period. In order to get better understanding of the data, we did XRD analysis over these samples to see the variation in the phases.

The XRD graphs of the sulfurized samples are shown in Figure 1.29 and 1.30. From the figure, we can see that the most prominent phase is $CuInS_2$ phase. The film has highly (112) oriented polycrystalline chalcopyrite phase. Figure shows the formation of In_5S_4 compound. There can be formation of CuxS compounds during the sufurization process which can be as a consequence of Cu-excess within the precursor layer. However, the Cu_xS phase is not seen in the XRD spectrum. It is expected to be present in this films on the surface of the film as discussed earlier.

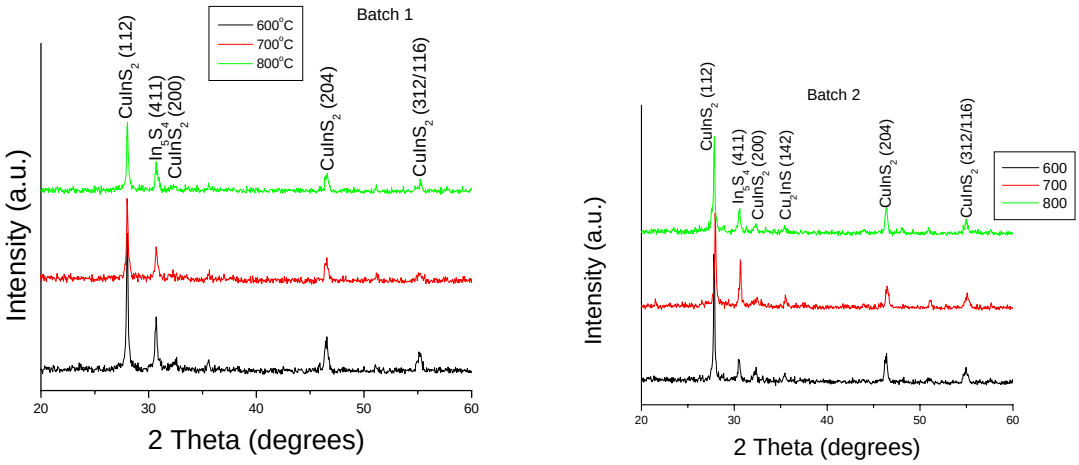

(a) (b)

Figure 1.29: XRD spectra of the samples after sulfurization. XRD spectra of evaporation (a) batch 1 and batch 2

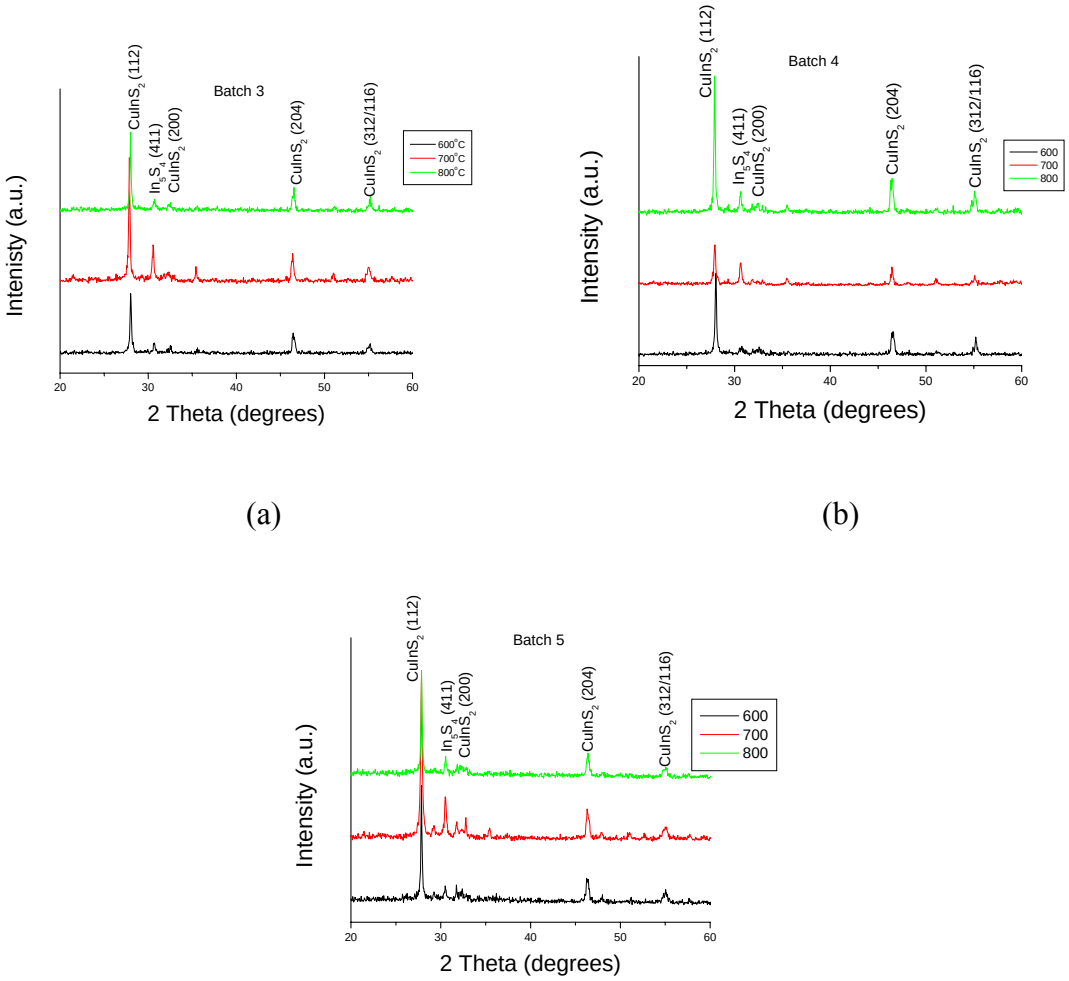

Figure 1.30: XRD spectra of the samples after sulfurization. XRD spectra of evaporation (a) batch 3, (b) batch 4, and (c) batch 5

However, from Figure 1.28 we see that even in In-rich films there is In loss occurring though the loss is comparatively very small.

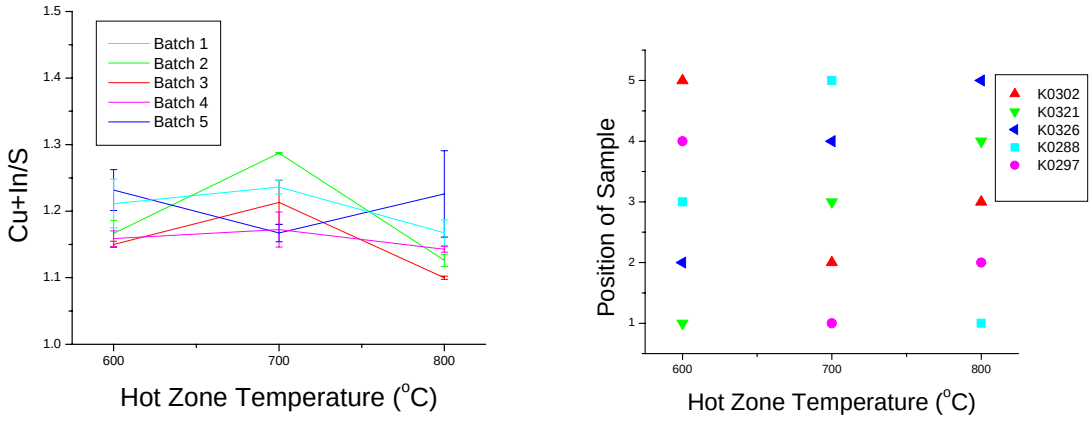

(a) (b)

Figure 1.31: (a) (Cu+In)/S ratio of the samples after sulfurization at 600, 700 and 800°C temperatures and (b) Location of samples during sulfurization

In Figure 1.31, the compositional analysis of the sulfurized samples are given along with the sample position during sulfurization. For film to be completely composed of $CuInS_2$, the (Cu +In)/S ratio needs to be 1.0. If the film were of CuS only, then the (Cu+In)/S ratio shall be 1.0. If the film were Cu_2S only, the (Cu+In)/S ratio would be 2.0. Hence, for a film that is composed of both the compounds, the (Cu +In)/S ratio needs to be between 1.0 and 2.0. From the figure 1.31(a), we can see the ratio is indeed great than 1.0 and lies between 1.1 and 1.3 reflecting $CuInS_2$ phase to be in the majority. The presence of Cu_2S and CuS phases has also been verified from the XRD spectra in Figure 1.31. Cu_2S and CuS phases are known to accumulate on the surface of the sulfurized film as discussed in section 1.1.3.

For the most of the samples with the 700 °C activation, the (Cu +In)/S ratio tends to rise and then fall again at 800 °C except for the sample from batch 5. Due to the strong

variation in the composition of the sample from batch 5, it is thought that the deviation observed is the artifact from the composition variation, which requires further investigation. More details of this will be discussed when we compare EDS results before and after KCN etching. XRD spectra shows that the relative formation of Cu_2S is more significant at 700 ^oC compared with the other temperatures. Also, strong presence of $CuInS_2$ can be seen at 800 ^oC.

For the In-rich samples, the location of sample does not have any direct effect on the quality of the film produced. There is less In-loss comparatively for the stoichiometric and the Cu-rich samples. We see that position of sample during sulfurization does not play any role for In-rich samples. For Cu-rich samples there is more significant In loss and it increases as the Cu concentration increases. We did not find any notable position effect on the composition of Cu-rich samples either.

The KCN etching was done on samples to remove Cu_xS compounds from the film which are expected to form on the surface of the film. 2 In-rich samples and 2 Cu-rich samples are subjected to etching to see the effect of etching on both kind of films. Hence, sample from batch 1 and batch 5 were subjected to ethcing They were sulfurized at HZ temperatures 700 ^oC and 800 ^oC respectively.

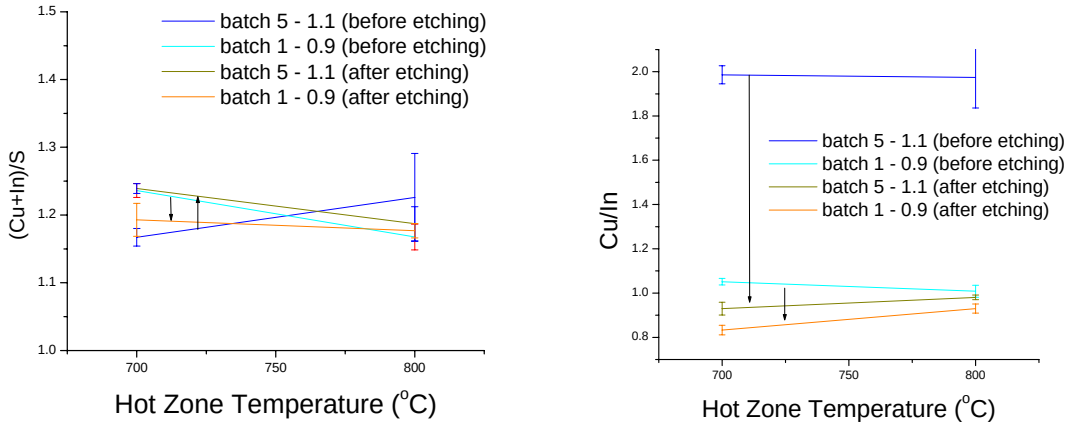

(a) (b)

Figure 1.32: (a) Cu to In ratio of the samples from batch 1 and batch 5 sulfurized at 700 °C and 800 °C. (b) (Cu+In)/S ratio of the samples from batch 1 and batch 5 at 700°C and 800°C. The composition after and before etching has been shown in the figures

From Figure 1.32(a), we see that there is significant reduction in Cu/In ratio for both samples – more reduction for batch 5 sample - reflecting that there was huge Cu_xS compound formation in the sample which was removed through KCN etching. This is consistent with what has been discussed in section 1.1.2. Figure 1.32(b) shows there is reduction in (Cu+In)/S ratio for the sample after etching. For the sample from batch 5, there was a large amount of variation in composition earlier before etching. However, after etching the variation is not there and the film is more homogenous in terms of concentration. For both samples, Cu/In ratio is more close to 1.0 at 800 °C. Also, the (Cu+In)/S ratio is close to 1.0 at 800 °C. From this, it is thought that more homogeneous $CuInS_2$ formation occurred at HZ temperature, 800 °C than 700 °C.

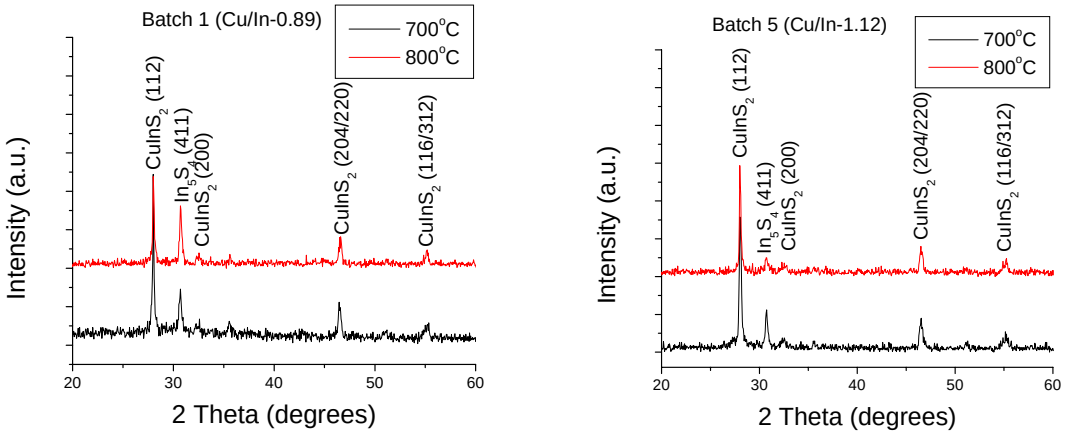

(a) (b)

Figure 1.33: XRD spectrum of the KCN etched samples from (a) batch 1 and (b) batch 5

Figure 1.33 shows that $CuInS_2$ is the primary compound after etching. Even after etching the In_5S_4 phase remains in the film. There is no significant change in the XRD spectrum after the etching. Hence, it can be deduced that the Cu_xS phase was present on the surface of the film which is removed by etching with KCN. In_5S_4 has been observed before to form during the sulfurization process [84]. This also explains the Cu to In ratio being less than one after KCN etching. We believe there was In_5S_4 compound formation during sulfurization.

1.4.1 Thermodynamic Calculations

We know that sulfur is present as S_8 at room temperature. However, at higher temperatures, lower molecular weight species are also available as described in the Introduction. Through the thermodynamic calculations, this study shows how much

reactive the smaller size sulfur molecules could be to some extent. For this, we find out the Gibbs free energy of formation of various compounds at 500^{o}C. Calculations are made at 500^{o}C since the substrate is kept at that temperature and most of the reactions will be taking at that temperature.

The standard formation enthalpy of $CuInS_2$ was assessed to be [82],

$$\Delta H^{o}_{298} = - 274.954.4 \pm 54.4 \text{ kJ/mol.}$$

Together with the standard entropy [99],

$$S^{o}_{298} = 136 \pm 0.8 \text{ J/mol K,}$$

the specific heat is given by

$$C_p = 94.68 + 2.794 \times 10^{-2} T - 5.364 \times 10^{5} T^{-2} \text{ J/mol K}$$

for the temperature range, 298 K< T < 500 K.

For the same temperature range, the free energy (kJ/mol) can be given as

$$G^{o} = (-306.1 \pm 54.4) + 0.5092 \times T - 1.397 \times 10^{-5} T^{2} - 0.09468 \times T \times \ln T + 268.2 T^{-1}.$$

Extrapolation to 773 K results in

$$Go = -407.207 \pm 54.4 \text{ kJ/mol.}$$

Table 5: Gibbs free energy function and standard enthalpy data for various species at 500 ^{o}C and at atmospheric pressure

Species	ΔH^{o}_{298} (kJ/mol)	$-(G^{o}_{T} - H^{o}_{298})/T$ (kJ/mol)
Cu (s)	0	0.041772
In (s)	0	0.07083
S_8 (g)	100.416	0.48673
S_2 (g)	128.576	0.23973

From the table 5, we calculate the Gibbs free energy formation of $CuInS_2$ for two different species of sulfur, S_8 and S_2.

$$4Cu(s) + 4In(s) + S_8(g) \rightarrow CuInS_2(s) \qquad \Delta G^{o}_{f} = 2.1629 \text{ kJ/mol}$$

$$Cu(s) + In(s) + S_2(g) \rightarrow CuInS_2(s) \qquad \Delta G^{o}_{f} = -10.0573 \text{ kJ/mol}$$

As the Gibbs free energy of formation of $CuInS_2$ is smaller and negative for S_2, we can say that there is more probability of forming $CuInS_2$ from S_2 specie than S_8 specie of sulfur. To be more precise, the calculation needs to be made for Cu-In compound instead of elemental metals. Due to the lack of availability of data the Gibbs free energy of formation of $CuInS_2$ with the Cu-In compounds was not able to be accomplished.

Table 6: Gibbs energy function and standard enthalpy data for various species at 500 ^{o}C and at atmospheric pressure

Species	ΔH^{o}_{298} (kJ/mol)	$-(G^{o}_{T} - H^{o}_{298})/T$ (kJ/mol)
In (g)	243	0.18108
In_2S (g)	138.072	0.33533
In_2S_2 (g)	22.32	0.34103

We also studied the possible mechanism of the loss of indium in the films. From Tables 5 and 6, we calculate the Gibbs free energy formation of In_2S and In_2S_2 gas species for two different species of sulfur.

$$16\ In(s) + S_8(g) \rightarrow 8\ In_2S(g) \qquad \Delta G^{o}_{f} = 22.8442 kJ/mol$$

$$4\ In(s) + S_2(g) \rightarrow 2\ In_2S(g) \qquad \Delta G^{o}_{f} = 90.4941\ kJ/mol$$

$$8\ In(s) + S_8(g) \rightarrow 4\ In_2S_2(g) \qquad \Delta G^{o}_{f} = -62.836\ kJ/mol$$

$$2\ In(s) + S_2(g) \rightarrow In_2S_2(g) \qquad \Delta G^{o}_{f} = -37.540\ kJ/mol$$

Also, we see the formation of In vapors from the In element:

$$In(s) \rightarrow In(g) \qquad \Delta G^{o}_{f} = 163\ kJ/mol$$

The simple calculation indicates Gibbs free energy of formation is negative only for the formation of In_2S_2 compound. Also, direct evaporation of elemental In is unlikely. It should be noted, however, the possible compound formation for In loss was predicted to be In_2S in earlier study [9]. Future study is further necessary to look at other possible mechanisms including decomposition of $CuInS_2$ and possible secondary indium sulfide

compounds – it was not clear from XRD, though, if the films have any secondary indium sulfide compounds.

1.5 CONCLUSION

Cu-In precursors were prepared on glass through evaporation of indium and copper elements sequentially on glass. Different compositions of Cu-In layers were prepared and analyzed for the phase formations in the film. $CuIn_2$ was found to be more prominent in the indium rich films and $Cu_{11}In_9$ was found to be dominating in copper rich films. The bilayers were sulfurized in a home built tube reactor under different Hot Zone conditions where sulfur vapor was thermally activated - cracked into smaller molecules. The sulfurized samples were analyzed for their composition and phase formations. The $CuInS_2$ film shows notable In loss and the strong presence of Cu_xS compounds in the film. The presence of Cu_xS phases was confirmed by KCN etching achieving Cu/In ratio close to 1. Higher concentration $CuInS_2$ phase was formed more at 800 ^oC than at 700 ^oC of HT Temperature after the EDS analysis from etching. From the thermodynamic calculation, it is shown that the $CuInS_2$ compound formation is from the copper and indium elements more probable with S_2 than S_8. The possible indium loss mechanism is predicted to be the formation of In_2S_2 compound if elemental indium is directly lost from the reaction with the two sulfur species.

CHAPTER 2

CADMIUM SULFIDE BUFFER LAYER FOR $CuInS_2$ SOLAR CELL

In this section, the experimental procedure, characterization technique and the result for the chemical bath deposited cadmium sulfide thin-film have been given. CdS layer has been studied since CdS layer is the typical n-type layer for the $CuInS_2$ p-n heterojunction solar cell. The CdS deposition setup was made in the lab to support the fabrication of the solar cells. The details of the setup have been discussed in this chapter. There is no new finding for this layer.

2.1 INTRODUCTION

Chemical bath deposition (CBD) technique was developed over 80 years ago for the production of PbS [85-87]. The first CdS films were made with this technique in 1960s [88] and CBD grown CdS thin films were used for $Cu(In,Ga)Se_2$ thin film solar cells for the first time in 1989 [89,90].

In CBD process, the chemical reaction of precursor species takes place in a liquid at a lower temperature (< 100 ^oC). CdS films are often formed by immersing a substrate in an alkaline aqueous solution (pH > 9) consisting of the following reactants:

1. a cadmium salt like $CdSO_4$, CdI_2, $Cd(CH_3COO)_2$
2. a complexing agent like NH_3, $N(CH_2CH_2OH)_3$
3. a sulfur precursor like $SC(NH_2)_2$, $SCNH_2CH_3$

Extensive studies on the growth kinetics and mechanism have been undertaken in the field [91-96]. The deposition rate and the film properties can be controlled by altering the temperature, pH, and the relative concentration of the chemical reactants in the solution [97]. Characteristic properties of CBD grown CdS thin films are following:

1. small grains (< 100 nm) [98].
2. possibility of coexistence of different crystal modifications like the würtzite hexagonal and the zincblend cubic structures [92,93].
3. very high resistivity (nearly intrinsic film).
4. high photosensitivity and long photocurrent decay times [99-101].
5. slight deviation from compositional stoichiometry due to the presence of impurity phases [102].
6. very thin films (< 50nm) [89].

2.2 EXPERIMENTAL PROCEDURE

2.2.1 Sample Preparation

As substrates, 3″ x 1″ size glass slides from Corning Glass Works (Cat. Number 2947) were used as substrates and they were cut into three 1”x1” pieces before use. Then, glass samples were cleaned in diluted Versa soap solution (Fisher). They were followed by further cleaning in the ultrasonic bath using toluene, acetone, and isopropyl alcohol for 20 minutes. The substrates were stored in tin boxed for later use.

2.2.2 Chemical bath setup and deposition

For the CBD, three different kinds of solutions were prepared:

Solution 1 ($CdSO_4$): A 250 ml Pyrex volumetric flask was rinsed with deionized (DI) water and filled halfway with DI water. 0.96 gm of $CdSO_4$ powder was broken up into large pieces and added to the volumetric flask. The solution was stirred to dissolve the powder and further diluted to 250 ml using DI water. The solution was then transferred to a Repipet dispenser.

Solution 2 ($SC(NH_2)_2$): A 500 ml Pyrex beaker was cleaned with DI water, and 14.25 g of thiourea powder was broken into smaller pieces and added to the beaker. DI water was added to the total volume 250 mL of Volumetric flask. A magnetic stir bar was kept in the beaker and the solution was stirred without heating until the thiourea was completely dissolved. The solution was then transferred to the a Repipet dispenser.

Solution 3 (NH_4OH): 30 vol% NH_4OH solution is prepared in a third Repipet dispenser.

All apparatuses were assembled and used under a fume hood. The substrates were prepared for the deposition by clipping two of them together back to back. A 250 ml beaker was filled with some amount of DI water, and the clipped samples were kept immersed in the water until other apparatus becomes ready. Another 250 ml reaction beaker was filled with 150 ml of DI water and 22 ml of solution 1 and 28 ml of solution 3 were added. A separate 30 ml beaker was filled with 22 ml of solution 2 and set aside. The reaction beaker was placed in a Pyrex dish filled with water (water bath), which had been already heated to 65 ^{o}C on a hot plate with the thermocouple in the water bath. The water level of the bath was about 5 - 10 mm from the top edge of the reaction beaker. As

soon as the reaction beaker was placed in the water bath, the substrates were placed in the reaction beaker, and the timer was started, all in rapid succession. The stir bar was placed inside reaction beaker stirring the solution at a moderate speed. After 1 minute has elapsed, the solution 2 was poured into the reaction beaker. The deposition was continued for extra 15 minutes. During the process, the temperature of the water bath was continuously monitored and controlled to maintain its temperature at 65 °C. As soon as the samples were removed, they were immediately rinsed under brisk stream of DI water. The samples were unclipped, blown dry with argon, and placed in a drying oven at 115 ^{o}C for 20 minutes. The samples were removed from the oven and stored.

The samples were characterized for their thickness using KLA Tencor profilometer. Opitcal transmittance measurements using Perkin Elmer UV-Visible-NIR spectroscope were also performed. Further details on the characterization tools and procedure can be found in Chapter 1.

2.3 RESULTS AND DISCUSSION

The samples prepared from the CBD process were characterized for their thickness and transmittance. The thickness for 15 minute deposition was discovered to be approximately 50 nm. Typically, the thickness of CdS film is kept below 50 nm because the series resistance of the cell becomes too big if CdS is too thick. Also, it has been reported the bandgap of the CdS thin-film decreases as the thickness increases [103]. The transmittance data of a sample is shown in figure 1.

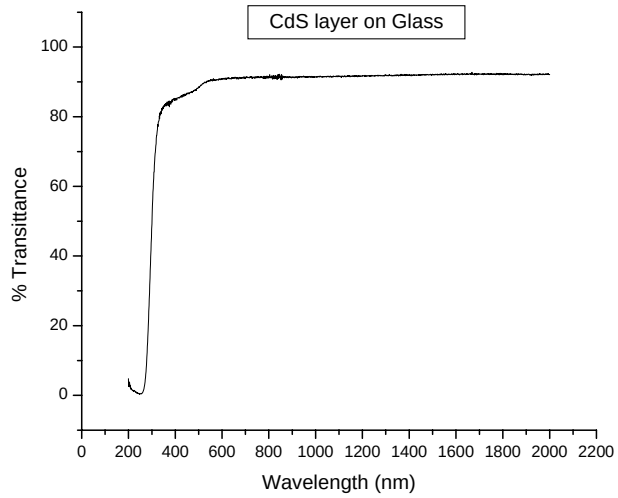

Figure 2.1: Percent transmittance of CdS layer on glass. Thickness is approximately 50 nm

From the figure, the transmittance is approximately 90 % over the spectral range measured. Higher transmittance in the visible range for CdS is desirable because light can be passed through CdS and be harvested by $CuInS_2$ layer. The transmittance falls slightly at about 500nm showing the interband absorption by the CdS layer. Similar patterns have been obtained which shows a bandgap of about 2.37 eV for CdS [104]. At about 320 nm, the transmittance drops down to zero showing the absorption by the glass. The interference fringes are not present in the data because the film is so thin that there are no interference fringes within the wavelengths used (200 - 2000 nm) and/or the film may be inconsistent in thickness preventing measurable interference.

2.4 CONCLUSION

CdS films were deposited on glass substrate using CBD technique. The films were characterized for their thickness and transmittance. The CdS film with thickness about 50 nm has been achieved and the film showed transmittance close to 90 % in the visible range.

CHAPTER 3

INDIUM TIN OXIDE WINDOW LAYER FOR $CuInS_2$ SOLAR CELL

Indium tin oxide (ITO) deposition has been studied as the part of the thesis research as it forms one of the layers of the cell. ITO is the window layer which primarily helps in the charge carrier collection from the CdS layer. It is transparent and colorless to allow light energy to reach $CuInS_2$ absorber layer. The ITO deposition by RF sputter has been optimized and the thin-film properties have been examined for the cell fabrication - the films deposited were characterized for their transmittance and sheet resistance.

3.1 INTRODUCTION

ITO thin films are typically deposited from a mixture of In_2O_3 and SnO_2, and ITO is a highly degenerate n-type semiconductor with a low electrical resistivity (0.005 -0.01 Ω·cm). The degeneracy is caused by both oxygen vacancies and substitutional Sn dopants created during film deposition. ITO is a wide band gap (E_g) semiconductor (3.5 - 4.3 eV), which shows high transmittance in the visible and near-IR regions of the electromagnetic spectrum. For high-quality ITO films, the transmittance is typically above 90 % in the visible range (400 - 700 nm). ITO films have a vast combination of technologically important properties: they have high luminous transmittance, high infrared reflectance, excellent substrate adherence, hardness, and chemically resistance [105]. The key material properties of ITO films are low resistivity (<200 μΩ-cm) and high transmittance

(90 %) in the visible light range. To date, many techniques have been developed to deposit ITO films including thermal evaporation [106], sputtering deposition with DC or RF power sources [107-109], chemical vapor deposition [110], and spray pyrolysis [111]. Various factors such as quality and reproducibility of the film, the cost and complexity of the equipment, and other advantages and disadvantages of a given method determine the choice of deposition technique.

ITO is widely used as a transparent conducting material in flat panel liquid crystal displays [112], electronic devices [113], solar cells [114], and antistatic coatings [115]. In particular, due to their high visible optical transmission and high electrical conductivity, ITO coatings are widely used as front or back contact electrodes for various thin film photovoltaic devices in substrate or superstrate configuration [116,117]. Also, they are being developed as transparent back contacts in new designs for bifacial and tandem thin films solar cells [118-120].

The properties of ITO films prepared from the RF sputtering are very much dependent on the deposition conditions, mostly on the substrate temperature and the distance between the target and the substrate. The effect of film thickness on the properties of ITO films has been studied as well [121-123].

3.2 EXPERIMENTAL PROCEDURE

3.2.1 Substrate Preparation

The substrate preparation is same as described in section 2.2.1.

3.2.2 Sputtering deposition

The RF sputter machine is used for the deposition of ITO on glass. The indium oxide - tin oxide target from Kurt J. Lesker is used which has 90 % In_2O_3 and 10 % SnO_2 by weight. The target has a copper backing plate which had been bonded using conventional indium bonding. The sputter gun underneath sample holder is inclined at an angle of 30° from the surface normal of the holder. The substrates were placed on the holder upside down. The target was continuously cooled with water which was flowing at the flow rate of 1.8 liter/minute. The temperature of the cooling water during the operation was kept under 30.6^{o}C. Argon was used as a working gas and the working pressure was controlled by a gate valve between a chamber and a cryo pump. Deposition was performed for various times to study the percent transmittance as a function of film thickness. Three batches of ITO deposition were conducted at different deposition time. The sputter conditions are summarized as follows:

Base Pressure: 10^{-7} torr range

Working Pressure: 2 x 10^{-3} torr

RF Power: 75 W (Forward), 0 W (Backward)

The films prepared by the RF sputtering were characterized for their properties. 4-point-probe was used to measure the sheet resistance of the film. The details of the four point probe were mentioned in section 1.3. UV-VIS spectrometer is used to measure the transmittance of the film whose details are also given in section 1.3. JEOL JEM 845 SEM is used to study the morphology of the film and XRD is used to confirm its crystal structure.

3.3 RESULTS AND DISCUSSION

It was observed that the sample placement on the holder inside sputter plays an important role in the thickness of the ITO film. Table 7 summarized the variation in the properties of samples from three different batches. The samples for each batch were placed at two different locations. Position 1 is the closer to the target while Position 2 is the farther from the target. The distance between the target and the Position 1 is 2.5″. There is no spacing in between the samples and the samples are placed next to each other. The target is inclined 30^{o} to the vertical.

Table 7: Variation of thickness and sheet resistance of ITO thin-films

Batch	**Position**	**Deposition time (minutes)**	**Thickness (nm)**	**Sheet resistance (Ω/square)**	**Resistivity (Ω-cm)**
1	1	90	568	45	0.0026
1	2	90	247	2160	0.0534
2	1	120	864	20	0.0063
2	2	120	688	653	0.0426
3	1	180	1350	13	0.0017
3	2	180	923	9310	0.0327

From Table 7, we can see that the thickness of the film increases as a function of deposition time in general. It can also be observed that the thickness varies as the position

changes. The samples from Position 1 are thicker while the samples from Position 2 are thinner, which is expected from the cosine distribution of ITO flux from the target. Another important characteristics is that the sheet resistance is lower for Position 1 than Position 2 regardless of the thickness of the sample.

The SEM picture of the ITO from batch 2 and position 2 is shown in Figure 3.2. The grain size ranges from 30 - 40 nm.

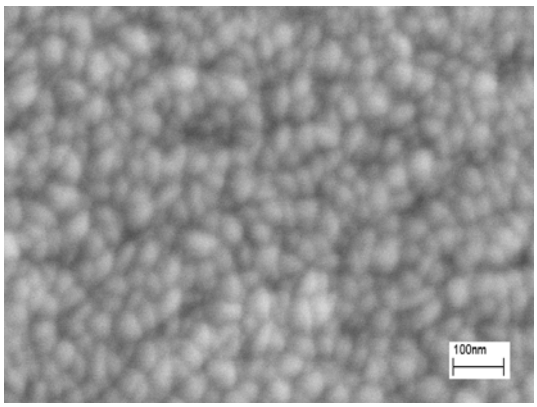

Figure 3.1: SEM graph of the ITO thin-film on glass. The grain size is around 40 nm.

3.4 CONCLUSION

ITO films with various thickness, ranging from 240 nm to 1350 nm, have been prepared by RF sputtering of ITO target under Ar atmosphere. The effect of sample position referenced to the target on the sheet resistance has been studied. For sheet resistance to be low, i.e. near 20 Ω/square, the position of the sample plays an important role. Also, the optical transmittance decreases as the ITO film thickness increases which is consistent with what other studies have observed [124].

CHAPTER 4

CONCLUSION

Cu-In precursors were prepared on glass through evaporation of indium and copper elements sequentially on glass. Different compositions of Cu-In layers were prepared and analyzed for the phase formations in the film. $CuIn_2$ was found to be more prominent in the indium rich films and $Cu_{11}In_9$ was found to be dominating in copper rich films. The bilayers were sulfurized in a home built tube reactor under different Hot Zone conditions where sulfur vapor was thermally activated - cracked into smaller molecules. The sulfurized samples were analyzed for their composition and phase formations. The $CuInS_2$ film shows notable In loss and the strong presence of Cu_xS compounds in the film. The presence of Cu_xS phases was confirmed by KCN etching achieving Cu/In ratio close to 1. Higher concentration $CuInS_2$ phase was formed more at 800 ^oC than at 700 ^oC of HT Temperature after the EDS analysis from etching. From the thermodynamic calculation, it is shown that the $CuInS_2$ compound formation is from the copper and indium elements more probable with S_2 than S_8. The possible indium loss mechanism is predicted to be the formation of In_2S_2 compound if elemental indium is directly lost from the reaction with the two sulfur species.

CdS films were deposited on glass substrate using CBD technique. The films were characterized for their thickness and transmittance. The CdS film with thickness

about 50 nm has been achieved and the film showed transmittance close to 90 % in the visible range.

ITO films with various thickness, ranging from 240 nm to 1350 nm, have been prepared by RF sputtering of ITO target under Ar atmosphere. The effect of sample position referenced to the target on the sheet resistance has been studied. For sheet resistance to be low, i.e. near 20 Ω/square, the position of the sample plays an important role.

REFERENCES

[1] Energy needs choices and possibilities, website of Royal Dutch/Shell, (2001).

[2] Granta, This overheating world, **83**, (2003).

[3] Ramanathan, K., Contreras, M.A., Perkins, C.L., Asher, S., Hasoon, F.S., Keane, J., Young, D., Romero, M., Metzger, W., Noufi, R., Ward, J., Duda, A., *Prog. Photovolt. Res. Appl*., **11**, 225-230 (2003).

[4] Probst, V., Stetter, W., Palm, J., Toelle, R., Visbeck, S., Calwer, H., Niesen, T., Vogt, H., Hernandez, O., Wendl, M., Karg, F.H., *Proceddings of the 3rd World Conference on Photovoltaic Solar Energy Conversion*, 329-334, Osaka, Japan (2003).

[5] S. M. Sze, Physics of Semiconductor Devices, Second Edition, 790, (1981).

[6] Siebentritt, S., *Solar Energy* **77**, 767-775, (2004).

[7] C. Dzionk, H. Metzner, H. Lewerenz, and H.-E. Mahnke, *J. Appl, Phys*., **78**, 2392, (1995).

[8] F. Adurodija, S. Kim, J. Song, K. Yoon, and B. Ahn, *Sol Energy Mater. Sol, Cells*, **55**, 225, (1998).

[9] C. Dzionk, H. Metzner, S. Hessler, and H.-E. Mahnke, *Thin Solid Films*, **299**, 38, (1997).

[10] A. Gupta, S. Shirakata, and S. Isomura, *Sol. Energy mater. Sol. Cells*, **32**, 137, (1994).

[11] D. Albin, J. Carapella, A. Duda, J. Tuttle, A. Tennant, and R. Noufi, in Twenty Second IEEE Photovoltaics Specialists Conference, Las Vegas, **2,** 907-913, (1991).

[12] R. Roy and S. Sen *J. Mater, Res*., **7**, 1377, (1992).

[13] J. Chen, El Kolawa, M.-A. Nicolet, and R. Ruiz, *Sol Cells*, **30**, 451, (1991).

[14] C. D. Lokhande and G. Hodes, S*ol Cells*, **21**, 215, (1987).

[15] B. M. Basol, V. K. Kapur, R. J. Matson, **CH2953**, 1179, (1991).

[16] A. Bolcavage, S. Chen, C. Kao, Y. Chang, and A. Romig, Jr., *J. Phase Equilib*, **14**, 14, (1993).

[17] H. Okamoto, *J. Phase Equilib*., **15**, 226, (1994).

[18] W. Keppner, T. Klas, W. Korner, R. Wesche, and G. Schatz, *Phys. Rev. Letter*., **54**, 2371, (1985).

[19] H. Metzner, M. Brussler, K.-D Husemann, and J.-J. Lewerenz, *Phys. Rev. B*, **44**, 11614, (1991).

[20] F. Weibke and H. Eggers, *Z. Anorg. Chem*., **220**, 273, (1934).

[21] T. P. Rajasekharan and K. Schubert*, Z. Metallkd*, **72**, 275, (1981).

[22] F. Laves and H. Wallbaum, *Z. Angew. Mineral*, IV, 17, (1941-1942).

[23] J. Reynolds, W. A. Wiseman, and W. Hume-Rothery, *J. Inst. Met*., **80**, 637, (1951-1952).

[24] K. C. Jain, M. ellner, and K. Schubert, *Z. Metallkd*., **63**, 456, (1972).

[25] A. Koster, L. Wolff, and G. Visser, *Acta Crystallogr. Sect*, B, **36**, 3094, (1980).

[26] Shay, J. L., Wernick, J. H., Ternary Chalcopyrite Semiconductor: Growth, Electric Properties and Applications, (1975).

[27] H. Goslowsky, S. Fiechter, R. Konenkamp, and H. J. Lewerenz, *Sol. Energy Mater*., **13**, 221, (1985).

[28] D. Cahen, Y. Mirowsky, and R. Tenne, *Solid State Chem*., **3**, 173, (1983).

[29] K. D. Husemann, PhD. Thesis, Technical University Berlin, Germany, (1991).

[30] H. J. Lewerenz, H. Goslowsky, and F. A. Thiel, *Sol Energy Mater*., **9**, 159, (1983).

[31] M. L. Fearheiley, N. Dietz, S. Schroetter, and J. J. Lewerenz, Proceedings of the International Conference on Advanced Materials, Symposium, Amsterdam, 125, (1992).

[32] N. Dietz, M. L. Fearheiley, and J. J. Lewerenz ibid, 133. Year?

[33] R. Hunger, R. Scheer, K. Diesner, and H. J. Lewerenz, *Appl. Phys. Lett*, **69**, 3010, (1996).

[34] D. S. Su, W. Newmann, R. Hunger, P. Schubert-Vischoff, M. Giersig, H. J. Lewerenz, R. Scheer, and E. Zeitler, *Appl. Phys. Lett*, **73**, 785, (1998).

[35] W. Calvet, PhD. Thesis, Brandenburgisch-Technical University Cottbus, Germany, (2002).

[36] M. Robbins, et al. J. Electrochem. Soc., **125**, 831, (1978).

[37] J. J. M. Bisnma. L.J. Giling, and J. Bloem, J. Crystal Growth, **50**, 429, (1980).

[38] J. J. M. Binsma, Ph.D. Thesis, Catholic University Nijmegen, Holland, (1981).

[39] H. J. Lewerenz and N. Dietz, *Appl. Phys. Lett*. **59**, 1470, (1991).

[40] H. J. Lewerenz and N. Dietz, *J. Appl. Phys*., **73**, 4975, (1993).

[41] J. J. M. Binsma, L. J. Giling, and J. Bloem, *J. Lumin*., **27**, 35, (1982).

[42] H. J. Lewerenz, *Solar Energy Materials & Solar Cells*, **83**, 400, (2004).

[43] M. C. Lux-Steiner, A. Ennaoui, C.-H. Fischer, A. Jager-Waldau, J. Klaer, R. Klenk, R. Konenkamp, T. Matthes, R. Scheer, S. Siebentritt, and A. Weideinger, *Thin Solid Films*, **533**, 361-362, (2000).

[44] Kai Siemer, Jo Klaer, Ilka Luck, Jurgen Bruns, Reiner Klenk, Dieter Braunig, *Solar Energy Materials & Solar Cells*, **67**, 159-166, (2001).

[45] J. Klaer, J. Bruns, R. Henninger, M. Weber, K. Ellmer, R. Klenk, R. Scheer, and D. Braunig, 14th European Photovoltaic Solar Energy Conference, Spain, 1307-1310, (1997).

[46] J. Klaer, J. Bruns, R. Henninger, K. Siemer, R. Klenk, K. Ellmer, and D. Braunig, *2nd Sci. Technol*., **13**, 1456-1458, (1998).

[47] S. Bandyopadhyaya, S. Chaudhuri, and A. K. Pal, *Solar Energy Materials & Solar Cells*, **60,** 323-339, (2000).

[48] Jerry D. Haris, Kulbinder K. Banger, David A. Scheiman, Mark A. Smith, Michael H.-C. Jin, and Aloysius F. Hepp, *Mat. Sci. and Engineering*, 150-155, **B98**, (2003).

[49] Christopher V Kelly, Michael H.-C. Jin, Kulbinder K. Banger, Jeremiah S. McNatt, John E. Dickman, and Aloysius F. Hepp, *Materials Science and Engineering,* **B 116**, 403-408, (2005).

[50] J. J. M. Binsma, and H. A. Van Der Linder, *Thin Solid Films*, **97**, 237-243, 1982.

[51] M. Gorska, R. Beaulier, J. J. Loferski, and B. Roessler, *Sol. Energy Mater*., **1**, 313, (1979).

[52] B. Pamplin and R. S. Feigelson, *Thin Solid Films*, **60**, 141, (1977).

[53] Jo Klaer, Ilka Luck, Axel Boden, Reiner, Klenk, Isabel Favilances Perez, and Roland Scheer, *Thin Solid Films*, **431-432**, 534-537, (2003).

[54] Ilka V. Luck, Jacobo Lvarez-Garcia, Lorenzo Calvo-Barrio, Axel Werner, Alejandro Perez-Rodriguez, J. R. Morante, and Dieter Braunig, *Mat. Res. Soc*, *Symp. Proc*, 668, (2001).

[55] W., Rosinger, M. Grade, W. Hirschwald, and Ber. Bunsenges, *Phys. Chem*., **87**, 536, (1983).

[56] D. Albin, J. Carapella, A Duda, J. Tuttle, A. Tennant, R. Noufi, and B. M. Basol, Proc. 22nd IEEE PVSC, IEEE (1991).

[57] R. Scheer, J. J. Lewerenz , *Journal of Vacuum Science and Technology*, **A 13 (4)**, 1924, (1995).

[58] R. Scheer, R. Klenk, J. Klaer, and I. Luck, *Solar Energy*, **77**, 777-784, (2004).

[59] R. Scheer, I. Luck, H. Sehnert, H. J. Lewerenz, H.J., *Solar Energy Materials and Solar Cells*, **41/42**, 261, (1996).

[60] R. Scheer, H.J. Lewernz, *Journal of Vacuum Science and Technology*, **A 12 (1)**, 51, (1994).

[61] M. Thackray, *Elemental Suflur*, Interscience, New York, 45, (1965).

[62] R. Steidel, *Elemental Suflur and Sulfur-Rich Compounds 1*, Springer, 54, (2003).

[63] H.-J. Mausle and R. Steudel, *Z. Anorg. Allg. Chem*., **478**,177,(1981).

[64] H. Braune and E. Steinbacher, Z. Naturforsch, Part A, 7, 486, (1952).

[65] P. Lenain, E. Picquenard, J. Corst, D. Jense, and R. Steudel, *Ber. Bunsenges. Phys. Chem.*, **92**, 859, (1988).

[66] E. Picquenard, O, El Jaroudi, and *J. Corset, J. Raman, Spectrosc*., **24**, 11, (1993).

[67] E. Picquenard, M. S. Boumedien, and J. Corset, *J. Mol. Stuct*., **293**, 63, (1993).

[68] M. S. Boumedien, J. Corset, and E. Picquenard, *J. Raman Spectrosc*., **30**, 463, (1999).

[69] H. Rau, T.R.N. Kutty, and J. R. F. Guedes de Carvalho, *J. thermoduy*., **5**, 833, (1973).

[70] F. Preuner and W. Schupp, *Z. Physik. Che*., **68**, 129, (1909).

[71] H. Braune, S. Peter, and V. Neveling, *Z. Naturforsch*. Part A, **6**, 32, (1951).

[72] H. Rau., T. R. N. Kutty, and J. R. F. Guedes de Carvalho, *J. Thermoduy*., **5**, 291, (1973).

[73] J. Berkowitz, and J. r. Marquart, *J. Chem. Phys*., **39**, 275, (1963).

[74] J. Berkowitz in Elemental Sulfur, Interscience, Publ., New York,; 125, (1965).

[75] D. Detry, J. Drowart, P. Goldfinger, H. Keller, and H. Rickert, *Z. Physik. Chem. NF*, **55**, 314, (1967).

[76] W., Rosinger, M. Grade, W. Hirschwald, and Ber. Bunsenges, *Phys. Chem*., **87**, 536, (1983).

[77] M. Weber, R. Scheer, H. J. Lewerenz, H. Jungblut, U. Storkel,, *Journal of the Electrochemical Society*, **149**, G77, (2002).

[78] JANAF Thermochemical Table, 3rd edn. [Chase M. W., Jr., Davies C. A., Downey J. r., Jr., Frurip D. J., McDonald R. A. and Syverud A. N., J. Phys. Chem. Ref. Data 14, Suppl. 1. (1985)], Amer. Chem. Soc. And Amer. Inst. Phys., New York, (1986).

[79] K. Mills, Thermodynamic Data for Inorg. Sulphides, Selenides and Tellurides. Butterwoth, London, (1974).

[80] R. Hultgren, R. L. Orr, P. D. Anderson and K. K. Kelley , Selected Values of Thermodynamic Properties of Metals and Alloys. Wiley, New York (1963).

[81] I. Barin and O. Knacke, Thermochemical Properties of Inorganic Substances. Springer, Berlin (1973).

[82] D. Cahen and R. Noufi, *J. Phys. Chem. Solids*, **53**, 991-1005, (1992).

[83] H. Migge, *J. Mater. Res*., **6**, 11, 2381-2386, 1991.

[84] C. Klopmann, J. Djordjevic, E. Rudigier, R. Scheer, *Journal of Crystal Growth*, **289**, 121, (2006).

[85] O. Hauser and E. Biesalski, *Chem. Zeitung*, **34**, 1079, (1910).

[86] F. Kicinksi, *Che. Indsutry*, **17**, 54, (1948).

[87] R. J. Cashman, *J. Opt. Soc., Am*., 36, 256, (1946).

[88] S. G. Mokrushin and Y. d. Tkachev, Kolloidn, zh., **23**, 438, (1961).

[89] R. W. Birkmire, B. E. McCandless, W. N. Shafarman, and R. D. Varrin, *Proceedings of the 9th European Photovoltaic Solar Energy Conference*, Freiburg, Germany, 134, (1989).

[90] R. H. Mauch, M. Ruckh, J. Hedstrom, D. Lincot, J. Kessler, R. Klinger, L. Stolt, J. Vedel, and H. W. Scholck, *Proceedings of the 10the E.C. Photovoltaic Solar Energy Conference*, Lisbon, Portuga, 1415, (1991).

[91] G. A. Kitaev and A. A. Uritskaya, Izvestriya Akademii Nauk *SSSR Neorganicheskie Materialy*, **2**, 1554, (1966).

[92] I. Kaur, D. K. Pandya, and K. L. Chopra, J. Electrochm. Soc., **127**, 943, (1980).

[93] T. L. Chu, S. S. Chu, N. Schultz, C. Wang, and C. Q. Wu, *J. Electrochm. Soc.*, **139**, 2443, (1992).

[94] R. Ortega-Borges and D. Lincot, *J. Eletrochem. Soc*., **140**, 3464, (1993).

[95] P. C. Rieke and S. B. Bentjen, *Chem. Mater*., **5**, 43, (1993).

[96] J. M. Dona and J. Herrero, *J. Electrochem. Soc*., **144**, 4081, (1997).

[97] Angela Kylner, Ph.D. Thesis, Uppsala University, Sweden, (1998).

[98] D. Lincot and R. Ortega-Borges, *Philosoph, Mag*, B, **68**, 185, (1993).

[99] P.K. Nair, J. Campos, M.T.S. Nair, *Semicond. Semicond. Sci. Technol*., **3**, 134, (1988).

[100] N. Pavaskar and C. Menezes, *Jpn. J. Appl. Phys*., **9**, 212, (1970).

[101] R. H. Bube, Photoelectronic Properties of Semiconductors, Cambridge University, (1992).

[102] R. Ortega-Borges, M. Froment, J. Vedel, and D. Lincot, *Solid State Phenomena*, **37-38**, 497, (1994).

[103] J.N. Ximello-Quiebras, G. Contreras-Puente, G. Rueda-Morales, O. Vigila, G. Santana-Rodri quez, A. Morales-Acevedo, *Solar Energy Materials and Solar Cells*, **90**, 727, (2006).

[104] Jae-Hyeong Lee, *Thin Solid Films*, **515**, 6089, (2007).

[105] Hamberg, H. Granqvist, C. G. *J. Appl, Phys*., **60**, R123, (1989).

[106] Paine, D. C. Whitson, T. Janiac, D. Beresford, R. and Yang, C., *J. Appl. Phys*, **85**, 8445, (1999).

[107] Hoon Yi, C. Shigesato, Y. Yasui, I. and Takakil, S., *J. Appl. Phys*. **34**, L244, (1995).

[108] Meng, L.-J. and Dos Santos, M. P., *thin Solid Films*, **289**, 65, (1996).

[109] Bender, M. and Trude, J., *Thin Solid Films*, **354**, 100, (1999).

[110] Kane, J. Scweizer, H. P. and Kern, W., *Thin Solid Films*, **29**, 155, (1975).

[111] Ramiah K. S., Raja V. S., Bhatnagar A. K., Tomlinson R. D., Pilkington R. D., Hill A. E., Chang S. J., Su Y.K., and Juang F.S., *Semi. Sci. Techn*, **15**, 676, (2000).

[112] R. Latz, K. Michael, and M. Scherer, *Jpn. J. Appl. Phys*., **30**, L149, (1991).

[113] J. S. Kim, M. Granstrom, and R. H. Friend, *J. Appl. Phys*., **84**, 6859, (1998).

[114] P. Topart, and P. Houquebie, *Thin Solid Films*, **352**, 243, (1999).

[115] Hamberg I., Granqvist C. G., *J. Appl. Phys*., **60**, 123, (1986).

[116] H. P. Lobl, M. Huppertz, and D. Mergel, Surf. Coat. Technol., **82**, 90, (1996).

[117] K. L. Chopra, P. D. Paulson, and V. Dutta, *Prog. Photovolt*: *Res. Appl*., **12**, 69, (2004).

[118] A. Romeo, M. Terheggen, D. Abou-Ras, D. L. Batzner, F. J. Haug, M. Kalin, D. Rudmann, and A. N. Tiwari, *Prog. Photovolt: Res. Appl*., **12**, 93, (2004).

[119] S. Nishiwaki, S. Siebentritt, P. Walk, and M. Ch. Lux-Steiner, *Prog. Photovolt: Res. Appl*., **11**, 243, (2003).

[120] T. Nakada, Y. Hirabayashi, T. Tokado, D. Ohmori, and T. Mise, *Sol Energy*, **77**, 739, (2004).

[121] A. N. Tiwari, G. Khrypunov, F. Kurdzesau, D. L. Batner, A. Romeo, and H. Zogg, *Prog. Photovlt: Res. Appl*., **12**, 33, (2004).

[122] H. Kim, J. S. Horwitz, G. Kushto, A. Pique, Z.H. Kafafi, C.M. Gilmore, and D. B. Chrisey, *J. Appl. Phys*, **88**, 6021, (2000).

[123] A. Guittoum, L. Kerkache, and A. Layadi, *Eur. Phys*. J., **7**, 201, (1999).

[124] Z. Qiao, R. Latz, and D. Mergel, *Thin Solid Fillms*, **466**, 250, (2004).

BIOGRAPHICAL INFORMATION

Karan Agrawal was born in Moradabad, India. He completed his Bachelor of Engineering in Chemical Engineering from Manipal Institute of Technology, Manipal, India. As a part of his curriculum, he conducted projects in Astra Zeneca Limited, Bangalore, India and in Indian Petrochemicals Corporation Limited, Baroda, India on the pollution in sewage water system.

In Fall 2005, he joined Materials Science and Engineering as a graduate student to obtain Master's Degree. He worked as a graduate research assistant in the Photovoltaics Materials Laboratory for two years. After completion of Master's degree, he will be joining Spansion Incorporation, Austin as the Wafer Fab Engineer.